A Two-Case Examination of the Synoptic and Mesoscale Processes Supporting Vertical Superposition of the Polar and Subtropical Jets over North America

By

ANDREW C. WINTERS and JONATHAN E. MARTIN*

Department of Atmospheric and Oceanic Sciences
University of Wisconsin-Madison
1225 W. Dayton St.
Madison, WI 53706
acwinters@wisc.edu

Keywords: Jet Streams; Ageostrophic Transverse Circulations; Convection
Running Head: Processes Supporting Jet Superposition

Submitted for publication in the *Quarterly Journal of the Royal Meteorological Society*
24 April 2015

* *Corresponding author address:* Jonathan E. Martin, Dept. of Atmospheric and Oceanic Sciences, University of Wisconsin-Madison, 1225 W. Dayton St., Madison, WI 53706. E-mail: jemarti1@wisc.edu

Abstract

Observational studies have shown that the tropopause characteristically exhibits a three-step pole-to-equator structure, with each break between steps in the tropopause height associated with a jet stream. While the two jet streams, the polar and subtropical jets, typically occupy different latitude bands, their separation can occasionally vanish, resulting in vertical superposition of the two jets. An examination of several historical and recent high-impact sensible weather events over North America suggests that superposed jets are an important component of their evolution. This study examines the processes that support the vertical superposition of the polar and subtropical jets during both the 18-20 December 2009 Mid-Atlantic Blizzard and the 1-3 May 2010 Nashville Flood.

Given that ageostrophic transverse circulations and convection have both been shown to be capable of restructuring the tropopause within a single jet environment, the analysis focuses on the role these same processes play within the more complex double jet environment. The results demonstrate that transverse circulations can play a dominant role in the production of superpositions by placing subsidence, and a downward protrusion of high potential vorticity air, between the two jet cores, thereby contributing to the production of the single, steep tropopause wall characteristic of the superposed jet environment. Furthermore, convection fundamentally influences the existence and structure of the subtropical jet stream, through both its associated latent heat release and irrotational outflow and the geostrophic adjustment process that responds to upper-tropospheric mass deposition from convection on the anticyclonic shear side of the jet.

1. Introduction

Narrow, rapidly flowing currents of air located near the tropopause are known as jet streams or jets. These jets, often found nearly girdling the globe while exhibiting large meridional meanders, are among the most recognizable structural characteristics within the Earth's atmosphere. Careful observational work by Defant and Taba (1957, hereafter DT57) was one of the first to demonstrate that the location of these jets is intricately related to the structure of the tropopause. Specifically, they found that the atmosphere is typically characterized by the three-step pole-to-equator tropopause structure[1] shown in Fig. 1 (modified from DT57, Fig. 13), wherein each step is separated from its neighbors by the presence of a westerly wind maximum. In particular, the subtropical jet typically resides within the break between the tropical (~90 hPa) and subtropical tropopause (~250 hPa) at the poleward edge of the Hadley cell (e.g., Loewe and Radok 1950; Yeh 1950; Koteswaram 1953; Mohri 1953; Koteswaram and Parthasarathy 1954; Sutcliffe and Bannon 1954; Krishnamurti 1961; Riehl 1962), while the polar jet is located farther poleward around 50^{o}N in the break between the subtropical tropopause and the even lower polar tropopause (~300 hPa). While relatively modest baroclinicity characterizes the subtropical jet in the upper troposphere and lower stratosphere, the polar jet sits atop the strongly baroclinic, tropospheric-deep polar front (e.g., Palmén and Newton 1948; Namias and Clapp 1949; Newton 1954; Palmén and Newton 1969; Keyser and Shapiro 1986; Shapiro and Keyser 1990).

A particularly insightful element of the DT57 analysis was their construction of hemispheric maps of tropopause height (in hPa). On these maps, one of which is shown in Fig. 2 (modified from DT57, Fig. 2), breaks in the tropopause, and thus the location of the respective jets at any particular time, are characterized by sharp, localized, and easily identifiable gradients

[1] DT57 identified the tropopause via the analysis of soundings. The tropopause was identified at the elevation of a "noticeable change of tropospheric lapse rate to an isothermal layer or to an increase of temperature with height." (DT57, p. 261)

in tropopause height. While such an analysis clearly demonstrates that both the polar and subtropical jets occupy different latitude bands, substantial meanders in their locations are common. Occasionally, the characteristic meridional separation between the two structures can disappear, as it does in Fig. 2 in the area bounded by the black circle over the North Atlantic, where the polar and subtropical jets vertically superpose. A consequence of such a vertical superposition of the two jets is the development of a two-step tropopause structure from the tropics to high latitudes, rather than the more common three-step structure represented in Fig. 1. More recently, potential vorticity (PV) tropopause maps have also been beneficial for identifying these breaks in the tropopause and the occasional vertical superposition of the polar and subtropical jets (e.g., Hoskins and Berrisford 1988; Davis and Emanuel 1991; Hakim et al 1995; Bosart et al. 1996; Morgan and Nielsen-Gammon 1998; Shapiro et al. 1999).

Employing companion maps of tropopause temperature (their Fig. 3), DT57 demonstrated that in the vicinity of a superposition the upper-tropospheric and lower-stratospheric baroclinicity associated with each jet individually is combined into a substantially narrower zone of contrast. Consequently, the associated superposed jet structure possesses an anomalous fraction of the pole-to-equator baroclinicity. Furthermore, the development of intensified baroclinicity associated with a superposed jet is often attended by a strengthening of its transverse, ageostrophic secondary circulation, diagnosable using the Sawyer-Eliassen circulation equation (Sawyer 1956; Eliassen 1962). These circulations are the primary dynamical mechanism by which superposed jets are involved in the production of sensible weather.

Recent work by Winters and Martin (2014) demonstrates one specific pathway through which the ageostrophic transverse circulation associated with a superposed jet can affect the evolution of a high-impact weather event. Their analysis showed that such a circulation contributed to the observed intensification of poleward moisture flux over the southeastern United States prior to the second day of heavy rainfall that characterized the 1-3 May 2010 Nashville Flood. Moore et al. (2012) explains that this increase in moisture flux was essential for the continued production of persistent heavy precipitation during the latter half of the event.

Superposed jets have also been linked, either directly or indirectly, to a number of other historical and recent high-impact sensible weather events at middle latitudes. Defant (1959) discussed the impact of a dramatic jet superposition on an explosive cyclogenesis event south of Iceland on 8 January 1956, in which the sea level pressure dropped 61 hPa in 24 h. Furthermore, the 25-26 January 1978 Cleveland Superbomb (Hakim et al. 1995; Hakim et al. 1996), the 15-16 October 1987 Great October Storm (Hoskins and Berrisford 1988), the 4-5 January 1989 ERICA IOP-4 storm (Shapiro and Keyser 1990), the 12-14 March 1993 Storm of the Century (Bosart et al. 1996), the 18-20 December 2009 Mid-Atlantic Blizzard (National Weather Service 2014), and the 25-28 April 2011 severe weather outbreak (Christenson and Martin 2012; Knupp et al. 2014) are all examples of events that occurred within an environment characterized by a jet superposition.

The association of jet superpositions with a class of high-impact sensible weather events motivates an investigation of the mechanisms that support the process of superposition. Historically, prior work that addresses the related topic of jet “mergers” has been focused on either interannual or climate time scales (e.g., Harnik et al. 2014), has been strongly based on wave-wave interaction (e.g., Lee and Kim 2003; Son and Lee 2005; Martius et al. 2010; O’Rourke and Vallis 2013), and/or has been conducted within an idealized model environment (e.g., Lee and Kim 2003; Son and Lee 2005; O’Rourke and Vallis 2013). This circumstance, coupled with only limited analysis of such features using actual observed data, has resulted in incomplete insight into the synoptic-dynamic mechanisms that foster the development of jet superpositions.

The concept of mid-latitude trough mergers (e.g., Lai and Bosart 1988; Gaza and Bosart 1990; Hakim et al. 1995; Hakim et al. 1996; Dean and Bosart 1996; Strahl and Smith 2001), in which two mid-tropospheric vorticity maxima with origins in distinctly different westerly airstreams amalgamate into a single maximum, offers the closest physical analog to jet superpositions in the synoptic-dynamic literature. These studies emphasize that trough merger often results in explosive cyclogenesis – also a frequent by-product of jet superposition. While it appears that certain trough merger cases may be simultaneously characterized by jet superpositions, the aforementioned studies do not identify the merging air streams as distinctly related to separate polar and subtropical jets and do not specifically investigate the impact of trough merger on the evolution of the upper-tropospheric jet and tropopause structure. Instead, the focus of these studies is largely placed on the effects merger can have on the development of surface cyclones.

Numerous observationally based studies have addressed the different mechanisms that can be responsible for altering the structure of an *individual* jet stream, however. For instance, the presence of ageostrophic transverse circulations, and particularly the differential vertical motions associated with them, in the vicinity of an upper-level jet-front system can act not only to aid in the production of sensible weather, but also to significantly restructure the baroclinicity and tropopause both above and below the jet. Many of the historical contributions to the problem of upper-tropospheric frontogenesis are well summarized by Keyser and Shapiro (1986), while Lang and Martin (2012) provide a recent extension of these studies to the process of lower-stratospheric frontogenesis.

The influence of convection in altering the structure of the tropopause on the anticyclonic shear side of a jet has also been well documented. In particular, Lang and Martin (2013) investigated four cases of upper-frontal evolution in southwesterly flow. They noted that latent heat release offers separate but simultaneous physical mechanisms that can alter the tropopause structure. First, direct diabatic erosion of PV above the heating maximum can increase the tropopause height in a given column. Second, the associated reduction in upper-tropospheric static stability intensifies the strength of an existing ageostrophic transverse circulation, which can then act to further tilt the tropopause. Tropical cyclones and extratropical transition events have also been shown to exert a considerable influence on the location and strength of the subtropical jet via their associated tropopause-level irrotational outflow (e.g., Archambault et al. 2013; Grams et al. 2013; Griffin and Bosart 2014).

Despite extensive research on a variety of aspects of upper-level jet-front systems, no prior study has examined the role of the above dynamical mechanisms in specifically supporting the interaction and subsequent vertical superposition of the two, initially distinct, jet features. Consequently, the present study will consider the specific roles that ageostrophic transverse circulations, convection, and the interaction of the two may play in the restructuring of the tropopause that characterizes jet superposition events.

These topics will be addressed through the examination of two recent high-impact weather events associated with jet superpositions: the 18-20 December 2009 Mid-Atlantic Blizzard and the 1-3 May 2010 Nashville Flood. These events were chosen because they occurred at different times of the year and were associated with different types of high-impact weather events (i.e., rapid cyclogenesis and an extreme precipitation event). Section 2 briefly discusses the identification criteria for the specific jet structures and provides some background on the Sawyer-Eliassen circulation equation, which is used to calculate the ageostrophic transverse jet circulations. Sections 3 and 4 focus on the development of a superposed jet during each individual case, respectively, and Section 5 finishes with a discussion and suggestions for future work.

2. Methodology

This study is performed using model analyses from the National Centers for Environmental Prediction (NCEP) Global Forecast System (GFS) at 6 h intervals with a horizontal grid spacing of 1.0^{o} x 1.0^{o} and a vertical grid spacing of 50 hPa (25 hPa between 1000 hPa and 900 hPa). To accommodate the jet identification scheme that follows, these data were bilinearly interpolated onto isentropic surfaces at 5-K intervals from 300-370-K using programs within the General Meteorological Package (GEMPAK; desJardins et al. 1991).

2.1 Jet Identification

The identification scheme for the polar, subtropical, and superposed jet streams is identical to that employed by Winters and Martin (2014), which is strongly based on the observational work by DT57 and is described with reference to the features shown in Fig. 3. Figure 3a depicts a characteristic example of clearly separate polar and subtropical jets in the eastern North Pacific. A vertical cross section through these distinct features unambiguously identifies the separate jet cores (Fig. 3b). From this cross section, it is clear that the core of the polar jet, located at approximately 300 hPa, is largely contained within the 315-330-K isentropic layer, while the subtropical jet core occupies the 340-355-K isentropic layer at roughly 200 hPa. Additionally, both the polar and the subtropical jets lie at the low PV edge of the strong horizontal PV gradient that separates the upper troposphere from the lower stratosphere in their respective layers. With these attributes in mind, the identification scheme identifies the presence, or absence, of a polar or subtropical jet within each grid column based upon the criteria specified in Winters and Martin (2014). The occurrence of both polar and subtropical jet characteristics in a single grid column identifies a jet superposition at that time in that grid column. An example of a jet superposition is shown in a plan view in Fig. 3c. Not until a vertical slice through the jet core is examined can the superposition be identified (Fig. 3d). Notice that, rather than the three-step tropopause structure identified by DT57 and shown in Fig. 3b, a superposed jet is characterized by a two-step tropopause structure with a steep tropopause wall that extends from the polar to the tropical tropopause. This nearly vertical PV wall (from roughly 550 to 150 hPa in this example case) is the leading structural characteristic of a superposed jet.

2.2 Sawyer-Eliassen Circulation Equation

A particularly powerful diagnostic tool for interrogating the ageostrophic transverse circulations associated with jet-front structures, in nearly straight flow, is afforded by the Sawyer-Eliassen circulation equation (Sawyer 1956; Eliassen 1962):

$$(-\gamma\frac{\partial\theta}{\partial p})\frac{\partial^2\psi}{\partial y^2}+(2\frac{\partial M}{\partial p})\frac{\partial^2\psi}{\partial p\partial y}+(-\frac{\partial M}{\partial y})\frac{\partial^2\psi}{\partial p^2}=Q_g-\gamma\frac{\partial}{\partial y}(\frac{d\theta}{dt}) \qquad (1)$$

where γ is a constant on isobaric surfaces [$\gamma=(R/fp_o)(p_o/p)^{c_v/c_p}$], p_o=1000 hPa, c_v=718 J kg^{-1} K^{-1}, c_p=1004 J kg^{-1} K^{-1}, R is the gas constant for dry air, θ is the potential temperature, and f is the Coriolis parameter. In addition, M is the absolute geostrophic momentum ($M=U_g-fy$), where U_g and V_g are the along- and across-front geostrophic winds, respectively, and Q_g is the geostrophic forcing term, which is the sum of the shearing {$Q_{SH}=2\gamma[(\partial U_g/\partial y)(\partial\theta/\partial x)]$} and stretching deformation terms {$Q_{ST}=2\gamma[(\partial V_g/\partial y)(\partial\theta/\partial y)]$}. The coefficients of the second-order terms on the left-hand side of (1) represent the static stability, baroclinicity, and inertial stability, respectively, and act to modulate the structure of the ageostrophic circulation. The ageostrophic circulation lies in a plane transverse to the frontal boundary (jet axis) and is determined by the Sawyer-Eliassen streamfunction, ψ, such that $v_{ag} = -\partial\psi/\partial p$ and $\omega = dp/dt = \partial\psi/\partial y$. For the purposes of this study, successive overrelaxation (SOR) is used to converge on a solution to (1) for the ageostrophic circulation following the method described by Winters and Martin (2014). The reader is referred to Eliassen (1962) or Keyser and Shapiro (1986) for the full derivation and a more detailed discussion of (1).

Employing (1), Shapiro (1982) described a series of conceptual models detailing the characteristic transverse circulations associated with idealized upper-level jet-front systems. Specifically, he demonstrated that, in the absence of any along-jet geostrophic temperature advection, solutions for the ageostrophic circulations are driven purely by the geostrophic stretching deformation and resembled the traditional four-quadrant model, with a thermally direct (indirect) circulation in the jet-entrance (-exit) region (Fig. 4a). The introduction of along-jet geostrophic temperature advection mobilizes the geostrophic shearing deformation term, which acts to "shift" the thermally direct (indirect) circulation to the anticyclonic (cyclonic) shear side of the jet in cases of geostrophic cold-air advection, such that subsidence is present through the jet core (Fig. 4b). Conversely, geostrophic warm-air advection along the jet axis shifts the thermally direct (indirect) circulation to the cyclonic (anticyclonic) shear side of the jet, positioning ascent through the jet core (Fig. 4c)[2].

3. Jet Evolution during the 18-20 December 2009 Mid-Atlantic Blizzard

3.1 Synoptic Overview

Throughout the 72 h period of 18-20 December 2009, large portions of the Mid-Atlantic and New England states accumulated 30-60 cm of snow in conjunction with a rapidly deepening

[2] These circulations are fortified by ascent and descent associated with positive and negative vorticity advection by the thermal wind (i.e., Sutcliffe 1947) as described by Martin (2014).

mid-latitude cyclone that formed over the northern Gulf of Mexico and tracked northeastward along the East Coast (Fig. 5; National Weather Service 2014). Coincident with the cyclone's most rapid period of intensification was the development of a jet superposition over the southeastern United States. For brevity, the following overview will focus primarily on the jet evolution in the upper troposphere in the hours preceding superposition.

At 0000 UTC 19 December, 36 h prior to jet superposition, a subtropical jet with winds in excess of 60 m s^{-1} extended from central Mexico northeastward across the Florida peninsula, while a weaker polar jet was identified upstream of a polar trough in northwesterly flow over the Central Plains (Fig. 6a). A cross section through the two separate jet structures at this time (Fig. 6b) indicates the presence of a three-step tropopause structure and demonstrates that the jets were clearly distinct from one another. The developing mid-latitude cyclone responsible for producing blizzard conditions across much of the eastern United States was also firmly located in a favorable position for further deepening in the subtropical jet's left exit region.

By 1800 UTC 19 December, the subtropical jet was displaced slightly poleward of its previous location and was noticeably stronger, with winds now in excess of 80 m s^{-1} (Fig. 6c). The surface cyclone, which had deepened by roughly 8 hPa, remained favorably located within the subtropical jet's left exit region off of the Mid-Atlantic coast, as well. Meanwhile, the polar jet, which was also characterized by increased wind speeds, had propagated around the base of the deepening polar trough and had assumed an orientation parallel to the subtropical jet over the southeastern United States. A cross section through the entrance regions of both of these jet structures (Fig. 6d) indicates the persistence of a three-step tropopause structure and that the two jets, while in closer proximity to one another by this time, were still not vertically superposed.

During the subsequent 18 h, the cyclone underwent its most rapid period of intensification, reaching a minimum central pressure below 980 hPa southeast of Cape Cod at 1200 UTC 20 December (Fig. 6e). Coincident with this period of most rapid intensification was a superposition of the polar and subtropical jets from central Georgia northeastward to off the North Carolina coast. This superposed jet was characterized by increased wind speeds, now well in excess of 90 m s^{-1}, and was positioned such that the cyclone was still firmly located in the jet's left exit region. An investigation of the movement of each individual jet axis from the previous time indicates that the subtropical jet was, once again, displaced only slightly poleward of its prior location, while the polar jet was located farther southeast of its previous position, consistent with the continued propagation and deepening of the polar trough.

A cross section drawn through the superposed portion of this jet illustrates the two-step tropopause structure and vertical PV wall (extending from roughly 500 hPa to 150 hPa) characteristic of a superposed jet (Fig. 6f). Consistent with this structure, the cross section no longer depicts two separate wind speed maxima, but rather a single jet core with wind speeds in excess of 90 m s^{-1}. Particular attention is drawn to the 320-K and 325-K isentropes, highlighted in red, which are located at a significantly lower altitude beneath the jet core than at the prior times (Figs. 6b,d). This suggests that subsidence was responsible for the downward depression of these isentropes during the intervening 18 h and, therefore, played a role in restructuring the tropopause into the characteristic superposed jet structure.

3.2 Superposed Jet Formation

Given that polar and subtropical jets are each associated with unique tropopause breaks, insight into the formation of a superposed jet can be garnered through a diagnosis of the movement of each individual tropopause break as they eventually become vertically aligned. In this case, the existence of a subtropical jet was closely tied to the presence of remote tropical convection over portions of Central America and the eastern equatorial Pacific Ocean. One particularly insightful way to examine the effect that tropical convection can have on the subsequent evolution of the subtropical jet is through a consideration of the anomalous pressure depth of the isentropic layer that contains the subtropical jet. Particularly telling is the depth of that layer on the anticyclonic shear side of the jet, where positive perturbation depths correspond to excess mass, relative to a long term mean, residing in the layer. The perturbation pressure depths of various isentropic layers are calculated as the difference between instantaneous pressure depths and a 31-yr (1979-2009) average depth at each grid point and analysis time, determined using NCEP's Climate Forecast System Reanalysis (CFSR) dataset (Saha et al. 2010). For the subtropical jet, we consider the pressure depth of the 340-355-K isentropic layer.

The outflow from tropical convection serves as one mechanism through which an isentropic layer can become anomalously inflated. Specifically, tropical convection often ingests boundary layer air with very high equivalent potential temperature (θ_e). Parcels embedded within convective updrafts are then exhausted at an isentropic level that roughly corresponds to this boundary layer θ_e. Often, such air is within the range of 340-355-K, coinciding with the isentropic layer that houses the subtropical jet. Furthermore, regions characterized by a strong horizontal gradient in perturbation pressure depth are associated with a perturbation geostrophic vertical shear, in accordance with the isentropic thermal wind relationship:

$$\frac{\partial \vec{V}_g'}{\partial \theta} = \frac{1}{\rho f \theta} \hat{k} \times \nabla p' \qquad (2)$$

Consequently, a subtropical jet is typically positioned on the poleward edge of an area characterized by positive perturbation pressure depths in the 340-355-K isentropic layer.

Figure 7a demonstrates that, at 0000 UTC 19 December, positive perturbation pressure depths in the 340-355-K isentropic layer were found over much of the Gulf of Mexico and Caribbean Sea on the anticyclonic shear side of the subtropical jet. Immediately upstream of the inflated isentropic layer were active areas of organized tropical convection over portions of the eastern equatorial Pacific Ocean and Central America (Fig. 7b), suggesting that convective outflow was a source of the excess mass found within the isentropic layer. Furthermore, the presence of weak, poleward-directed divergent winds acting on the subtropical tropopause break (red dashed line) encouraged a slight poleward shift in the location of the subtropical jet, consistent with the observations made from Figs. 6a,c.

At 1800 UTC 19 December, perturbation pressure depths increased in both magnitude and areal coverage over a large portion of the central Caribbean and off the southeastern United States coast and maintained an association with convection in the tropics (Figs. 7c,d). Figure 7c also identifies that weak, poleward-directed divergent winds persisted in the vicinity of the subtropical tropopause break, which continued to support a slight poleward shift of the subtropical jet's axis. Figure 7e demonstrates that this subtle poleward shift in the location of the subtropical jet continued up until 1200 UTC 20 December when the polar and subtropical jets superposed. Furthermore, coincident with the jet's increased wind speed is a strengthened gradient in perturbation pressure depth immediately equatorward of the jet axis from the eastern Gulf of Mexico northeastward towards Bermuda.

The upper-tropospheric evolution in the hours preceding superposition strongly suggests that persistent remote tropical convection over the eastern equatorial Pacific Ocean and Central America was responsible for an inflation of the 340-355-K isentropic layer. Trajectory analysis, using the NOAA/ARL HYSPLIT model (Draxler and Hess 1997; Draxler and Rolph 2015;

Rolph 2015), of parcels originating in the vicinity of the tropical convection at 1200 UTC 18 December (Fig. 8) confirms this assertion, with roughly a quarter of the trajectories characterized by rapid ascent in the 12-24 h following their initiation and warming to potential temperatures of 340-350-K. Upper-tropospheric southwesterly flow downstream of the low-latitude trough west of Mexico then acted to transport the convective outflow towards the Caribbean Sea in the 24-36 h prior to superposition, resulting in the positive perturbation pressure depths observed there. Consequently, there is strong evidence that the combination of both persistent tropical convection and the approach of a low-latitude trough contributed to the existence of the subtropical jet. First, by facilitating an inflation of the 340-355-K isentropic layer in the tropics and, secondly, by the subsequent translation of mass within that layer towards higher latitudes.

Focusing attention on the evolution of the polar jet, and its interaction with the subtropical jet, Fig. 9a shows that the polar jet sat atop a region of enhanced baroclinicity that extended from northwestern Kansas southeastward into northern Mississippi at 0000 UTC 19 December. Furthermore, the geostrophic jet exit region was characterized by weak geostrophic cold air advection over southern Missouri and northern Arkansas. This suggests, based on Shapiro's (1982) conceptual model, that the transverse ageostrophic circulation associated with the polar jet's exit region was shifted relative to the jet axis such as to position descent through the jet core. The solution for the Sawyer-Eliassen circulation within the cross section identified in Fig. 9a confirms this notion, depicting a region of subsidence centered squarely beneath the polar jet core (Fig. 10a). This subsidence was driven by the presence of dipole circulations, which consisted of a thermally direct (indirect) circulation to the south (north) of the jet core. Specifically, this subsidence was not only responsible for strengthening the mid-tropospheric temperature gradient via tilting, but also for supporting a downward protrusion of high PV air associated with the development of the polar tropopause fold.

By 1800 UTC 19 December, the polar jet had propagated around the base of the polar trough and assumed an orientation parallel to the axis of the subtropical jet over the southeastern United States (Fig. 9b). Furthermore, geostrophic wind speeds associated with the polar jet increased to greater than 60 m s^{-1}, in response to the intensified horizontal baroclinicity situated beneath the jet. The magnitude of the geostrophic cold air advection also strengthened further from the prior time in the vicinity of both jets' entrance regions over northern Alabama, suggesting continued subsidence in the vicinity of the jet cores.

The Sawyer-Eliassen circulation within the cross section G-G', drawn through the entrance region of both the polar and subtropical jets at this time, is characterized by a strong thermally direct circulation with subsidence confirmed directly on and beneath the subtropical tropopause step[3] (Fig. 10b). Consequently, this subsidence was favorably positioned to advect high PV air downward and to lower the altitude of the subtropical tropopause step with time. From another perspective, it is apparent that the 320-K and 325-K isentropes were situated within the horizontal baroclinicity that sat beneath the subtropical jet. The presence of a mid-tropospheric maximum in subsidence through the polar jet core, as indicated in Fig. 10b, implies that the 320-K isentrope was advected downward on the poleward side of the subtropical jet at a more rapid rate than the 325-K isentrope, reducing the horizontal baroclinicity beneath the subtropical jet. At the same time, the subsidence acted to incorporate these same isentropes into a strengthening region of baroclinicity beneath the polar jet core (Fig. 6f). Consequently, the subsidence associated with the Sawyer-Eliassen circulation promoted an intensification of the

[3] Cross sections along the entire length of the polar and subtropical jets are consistent with the result shown in Fig. 10b.

baroclinicity directly beneath the polar jet core at the expense of the subtropical jet's baroclinicity and, subsequently, the production of one consolidated region of intense horizontal temperature contrast that is characteristic of a superposed jet.

By 1200 UTC 20 December, the polar tropopause break became vertically aligned with the subtropical tropopause break, producing the vertical PV wall shown in Fig. 6f and a superposed jet from central Georgia northeastward to eastern North Carolina (Fig. 9c). Wind speeds in the core of the superposed jet increased as well, consistent with the consolidation of baroclinicity beneath the superposed jet. Notably, locations upstream of the superposed jet remained characterized by strong geostrophic cold air advection, indicating continued forcing for subsidence on and beneath the subtropical tropopause step and supporting the development of the two-step tropopause structure observed downstream.

Overall, this case is one in which the production of a jet superposition is most strongly driven by the effects of internal jet dynamics. While the convection over Central America and the equatorial Pacific Ocean was essential for strengthening and establishing the subtropical jet, it only promoted a slight poleward shift in the location of the jet axis. Ageostrophic transverse circulations, on the other hand, were crucial, not only in the production of a polar tropopause fold, but also in driving a downward protrusion of high PV air centered squarely on the subtropical tropopause step. It appears that these vertical motions, which were present along the entire length of the subtropical tropopause step between the polar and subtropical jet axes 18 h prior to superposition, were primarily responsible for reshaping the tropopause into the characteristic two-step structure associated with a superposed jet.

4. Jet Evolution during the 1-3 May 2010 Nashville Flood

4.1 Synoptic Overview

The 1-3 May 2010 Nashville Flood was an historic two-day event in which two consecutive mesoscale convective systems (MCSs) were responsible for rainfall accumulations in excess of 180 mm (7 in.) across a large portion of Tennessee, southern Kentucky, and northern Mississippi (Fig. 11). Moore et al. (2012) and Durkee et al. (2012) provide excellent overviews of both the meso- and synoptic-scale processes responsible for the production of precipitation in this case and the reader is referred to those works for any additional information. As with the December 2009 case, here we present an abbreviated synoptic overview that focuses solely on the jet evolution in the upper troposphere during the 24 h period of 0000 UTC 1 May 2010 - 0000 UTC 2 May 2010 across the contiguous United States.

Figure 12a depicts a high amplitude flow pattern in place over a large portion of North America at 0000 UTC 1 May, with a deep, positively tilted trough over the western United States and a strong ridge over the east. A polar jet was identified downstream of the trough axis and extended from Baja California northeastward into the Central Plains, while a subtropical jet, which was of comparable strength to the polar jet, stretched from northern Mexico eastward along the Gulf Coast. Note that at this time, even though the two jets are in close proximity to one another, they are not superposed. A cross section through the two separate jet cores (Fig. 12b) confirms this diagnosis and depicts a clear, three-step tropopause structure with each tropopause break associated with a distinct wind speed maximum.

At 1200 UTC 1 May, a broad area of precipitation situated over much of the Ohio River Valley helped to further build the extensive ridge that was in place over a large portion of the eastern United States. Consequently, in response to the strengthened ridge, the axis of the subtropical jet shifted noticeably poleward and westward, bringing it closer to the polar jet (Fig. 12c). A cross section through the two jet structures at this time illustrates that a three-step tropopause structure remained intact, while clearly showing the movement of the subtropical jet towards the northwest and a wind speed increase in both jets (Fig. 12d).

At 0000 UTC 2 May, the polar and subtropical jets became superposed over portions of west Texas and southwestern Oklahoma, as the axis of the subtropical jet continued to migrate towards the northwest and the western trough shifted slowly eastward (Fig. 12e). A cross section through the superposed portion of the jet (Fig. 12f) shows both the appearance of a slight equatorward shift in the location of the polar tropopause break within the plane of the cross section and the continued northwestward migration of the subtropical tropopause break, which combined to produce the two-step tropopause structure and vertical PV wall characteristic of a superposition. Further note that the two wind speed maxima are now consolidated into a single jet core that featured wind speeds greater than 70 m s^{-1}, in response to the increased horizontal baroclinicity in the upper troposphere and lower stratosphere that accompanied the superposition.

4.2 Superposed Jet Formation

At 0000 UTC 1 May, the polar jet sat atop a rather extensive and continuous area of mid-tropospheric baroclinicity that stretched from just off the coast of southern California into northern Minnesota (Fig. 13a). Furthermore, the jet entrance region of the polar jet was characterized by an area of geostrophic cold air advection centered squarely in the base of the western trough. As in the December 2009 case, Shapiro’s (1982) conceptual model implies that this forcing will act to promote subsidence beneath the jet core, this time by shifting the thermally direct circulation in the entrance region towards the anticyclonic shear side of the jet (Fig. 4b).

The Sawyer-Eliassen circulation within the cross section identified in Fig. 13a conforms to this idealized model, placing subsidence directly beneath the polar jet core and in the vicinity of the polar tropopause fold (Fig. 14). This subsidence, once again, acts both to drive a downward protrusion of high PV air into the middle troposphere and to increase the horizontal baroclinicity beneath the jet via tilting. Subsequently, regions of strong mid-tropospheric baroclinicity in Figure 13 correspond roughly to the location of the polar tropopause fold. It is also likely that curvature effects associated with the western trough further enhanced the total subsidence observed in the jet entrance region beyond that estimated by the transverse circulation (not shown). Consequently, it is conceivable that flow curvature, in addition to the diagnosed transverse circulation, acted to accentuate the development of the polar tropopause fold in this location and to strengthen the polar jet.

At 1200 UTC 1 May, the axis of the polar jet became fractured near the United States/Mexico border (Fig. 13b), presumably under the influence of ongoing convection over the southern Mississippi River Valley. Additionally, locations in the vicinity of the jet fracture were characterized by an environment favorable for large-scale ascent, given the close proximity of the upstream trough, which decreased the horizontal temperature gradient in the middle troposphere via tilting downstream of the Rio Grande. Further upstream, in the base of the trough, geostrophic jet wind speeds increased from the previous time in response to the strengthened baroclinicity beneath the jet. Geostrophic cold air advection remained strong in the base of the trough at this time as well, suggesting continued subsidence in the vicinity of the polar jet core and the subsequent maintenance of the polar tropopause fold.

At 0000 UTC 2 May, the polar jet streak in the base of the trough was positioned slightly downstream of its previous location, such that its most downstream edge overlapped with the region of superposition identified in Fig. 12e over southwestern Oklahoma and west Texas (Fig. 13c). Furthermore, rather intense baroclinicity, which extended from the Southern Plains upstream to Baja California, continued to characterize the polar jet streak. Recalling that this area of baroclinicity was also associated with the development of a polar tropopause fold, it becomes clear that the appearance of an equatorward displacement of the polar tropopause break within Figs. 12d,f is simply the downstream propagation of an intense polar tropopause fold into the area of superposition, as the trough slowly migrated eastward.

As suggested, the evolution of the subtropical jet is closely tied to the persistent convection present over portions of the southern Mississippi River Valley throughout the duration of the flooding event. Recall that at 0000 UTC 1 May the subtropical jet was characterized by a rather zonal orientation and was distinct from the polar jet (Fig. 12a). Furthermore, Fig. 15a depicts a minimum in velocity potential at 200 hPa (approximately the level of maximum divergent outflow) centered along the Mississippi River Valley, consistent with the presence of large-scale ascent in that location, and a maximum in velocity potential immediately upstream of the trough over the western United States. The juxtaposition of these two features resulted in the presence of easterly divergent winds over the spine of the Rocky Mountains and northern Mexico. At this time, these divergent winds were responsible for only a weak region of negative PV advection over northern Mexico along the subtropical tropopause break, given its rather zonal orientation.

By 1200 UTC 1 May, it is apparent that latent heating from the ongoing convection over the southern Mississippi River Valley had acted to significantly erode upper tropospheric PV in that location, as demonstrated by the poleward retreat of the 1- and 2- PVU contours at 200 hPa (Fig. 15b). Consequently, the subtropical jet became characterized predominantly by southwesterly flow and took on an orientation that was roughly parallel to the polar jet. Divergent winds across northern Mexico also strengthened considerably over the previous 12 h, largely due to the enhanced outflow from convection over portions of Tennessee and southern Kentucky. The combination of these two factors resulted in a significantly more favorable situation for the divergent winds to displace the subtropical tropopause break towards the northwest, as indicated by the increase in negative PV advection along the subtropical tropopause break. This northwestward trend in the position of the subtropical jet axis, driven by the convective outflow, continued up until 0000 UTC 2 May, when it vertically superposed with the polar jet axis over portions of west Texas and southwestern Oklahoma (Fig. 15c).

In contrast to the December 2009 case, jet superposition in the May 2010 case was predominantly driven by the presence of convection over the southeastern United States. The analysis demonstrates that the convection acted to substantially restructure the tropopause via 1) the diabatic erosion of upper-tropospheric PV and, 2) advection of the subtropical jet axis westward towards the polar jet via its associated divergent outflow. However, much like the December 2009 case, persistent geostrophic cold air advection in the base of the western trough drove an area of subsidence in the vicinity of the polar jet core and facilitated the development of a tropopause fold. This fold subsequently propagated downstream into west Texas and southwestern Oklahoma by 0000 UTC 2 May where it undercut the retreating subtropical tropopause break, thereby facilitating the development of the superposed jet structure.

5. Discussion

Motivated by the identification of jet superpositions in several historic and recent high-impact sensible weather events, this study examines the dynamical processes responsible for producing a superposition during the 18-20 December 2009 Mid-Atlantic Blizzard and the 1-3

May 2010 Nashville Flood. The two cases selected highlight the fact that jet superpositions can be associated with different types of sensible weather events and can develop at different times of year. Given that ageostrophic transverse jet circulations and convection both influence the restructuring of the tropopause within single jet environments, the analysis focuses on the role these same mechanisms play in reshaping the tropopause within the more complex double jet environment.

Both cases were characterized by mid-tropospheric geostrophic cold air advection in cyclonic shear along a portion of the polar jet at some point prior to superposition, indicating that subsidence was positioned directly through and beneath the polar jet core. Consequently, the descending motions were favorably positioned to facilitate downward advection of high PV air from the stratosphere and to contribute to the requisite restructuring of the tropopause that characterizes a jet superposition. In the December 2009 case, this subsidence was specifically positioned directly on and beneath the subtropical tropopause step and in the immediate vicinity of both the polar and subtropical jets. Consequently, the subsidence was instrumental in lowering the tropopause height in the region between the two individual jets and for consolidating the baroclinicity associated with each jet into one single zone of contrast. For comparison, only the jet entrance region of the polar jet was associated with subsidence during the May 2010 Flood. As a result, the subsidence in that case only fostered the development of a polar tropopause fold, instead of working to directly assimilate the two jets into a single structure.

The two cases examined as part of this study also demonstrate the different roles that convection can play in facilitating a superposition. For instance, during the May 2010 Flood, convection occurred in the immediate vicinity of the subtropical jet. This convection subsequently acted to restructure the tropopause via material displacement and diabatic erosion of upper-tropospheric PV. Conversely, the December 2009 case was associated with remote convection that occurred in the tropics. This tropical convection was primarily responsible for substantially enhancing the subtropical jet by inflating the anticyclonic shear side of the isentropic layer containing the jet. Together, these two cases demonstrate that the proximity of convection to the jet structure may determine the nature of its influence on the jet. For example, proximate convection can have a rapid local, yet transient impact on the jet structure through its divergent outflow and latent heat release. Alternatively, remote convection can drive a slower acting, but persistent impact via the development of what might be termed tropical tropopause anticyclones – the balanced response to upper-tropospheric mass deposition on the anticyclonic shear side of the subtropical jet.

While both cases illustrate that internal jet dynamics and convection can play important roles in the development of a superposition, it is clear that the individual importance of each component to the process of jet superposition depends on the case being considered. For instance, it appears that internal jet dynamics played a more prominent role during the December 2009 case, while convection was the dominant component during the May 2010 Flood. A broader survey of jet superposition events over North America may help 1) to pinpoint the environmental characteristics most conducive for the development of superpositions and 2) to determine whether or not that preferred environment varies seasonally or geographically.

Another particularly useful way to investigate the physical processes involved in jet superpositions is found by employing piecewise PV inversion techniques (e.g., Hoskins et al. 1985; Davis and Emanuel 1991). As a product of ongoing work, we have developed a scheme that isolates the individual PV anomalies associated with each jet structure by considering the distribution of PV within isentropic layers characteristic to each jet. A prominent outcome that emerges from an inversion of these PV anomalies, as well as those generated diabatically from convection, is an ability to diagnose both the lateral and vertical interactions between separate PV anomalies within a double jet environment and to assess the individual role that each anomaly plays in restructuring the tropopause during the process of superposition.

Finally, persistent observation of these structures by the authors throughout the development of this study has made clear that significant sensible weather is not tied to every jet superposition event. Consequently, greater knowledge regarding the environmental differences that exist between null cases and those associated with significant sensible weather over North America remains outstanding. The ability to diagnose the formation of these structures, and to understand the specific role they can play in the development of sensible weather at middle latitudes, has important implications for short-term weather prediction. This knowledge may further lead, depending on the degree to which these structures can be identified within climate models, to an increased capability for interrogating the nature of the jet structure within a future climate.

Acknowledgments

This work was supported by the National Science Foundation through grant NSF-1265182.

References

Archambault, H. M., L. F. Bosart, D. Keyser, and J. M. Cordeira, 2013: A climatological analysis of the extratropical flow response to recurving western North Pacific tropical cyclones. *Mon. Wea. Rev.,* **141,** 2325-2346.

Bosart, L. F., G. J. Hakim, K. R. Tyle, M. A. Bedrick, W. E. Bracken, M. J. Dickinson, and D. M. Schultz, 1996: Large-scale antecedent conditions associated with the 12-14 March 1993 cyclone ("Superstorm '93") over eastern North America. *Mon. Wea. Rev.*, **124,** 1865-1891.

Christenson, C. E., and J. E. Martin, 2012, March: The large-scale environment associated with the 25-28 April 2011 severe weather outbreak. *16th NWA Severe Storms and Doppler Radar Conference*, Des Moines, IA, National Weather Association, 31 March 2012.

Draxler, R. R., and G. D. Hess, 1997: Description of the HYSPLIT_4 modeling system. NOAA Tech. Memo. ERL ARL-224, NOAA Air Resources Laboratory, Silver Spring, MD, 24 pp.

———, and G. D. Rolph, 2015: HYSPLIT (Hybrid Single-Particle Lagrangian Integrated Trajectory) Model access via NOAA ARL READY Website (http://ready.arl.noaa.gov/HYSPLIT.php). NOAA Air Resources Laboratory, Silver Spring, MD.

Davis, C. A., and K. E. Emanuel, 1991: Potential vorticity diagnostics of cyclogenesis. *Mon. Wea. Rev.*, **119,** 1929-1953.

Dean, D. B., and L. F. Bosart, 1996: Northern Hemisphere 500-hPa trough merger and fracture: A climatology and case study. *Mon. Wea. Rev.,* **124,** 2644-2671.

Defant, F., 1959: On hydrodynamic instability caused by an approach of subtropical and polarfront jet stream in northern latitudes before the onset of strong cyclogenesis. *The Atmosphere and Sea in Motion,* New York, Rockefeller and Oxford University Presses, 305-325.

———, and H. Taba, 1957: The threefold structure of the atmosphere and the characteristics of the tropopause. *Tellus*, **9,** 259-275.

desJardins, M. L., K. F. Brill, and S. S. Schotz, 1991: Use of GEMPAK on UNIX workstations. Preprints, *Seventh Int. Conf. on Interactive Information and Processing Systems for Meteorology, Oceanography, and Hydrology,* New Orleans, LA, Amer. Meteor. Soc., 449-453.

Durkee, J. D., L. Campbell, K. Berry, D. Jordan, G. Goodrich, R. Mahmood, and S. Foster, 2012: A synoptic perspective of the record 1-2 May 2010 mid-South heavy precipitation event. *Bull. Amer. Meteor. Soc.*, **93,** 611-620.

Eliassen, A., 1962: On the vertical circulation in frontal zones. *Goephys. Publ.*, **24,** 147-160.

Gaza, R. S., and L. F. Bosart, 1990: Trough merger characteristics over North America. *Wea. Forecasting*, **5,** 314-331.

Grams, C. M., S. C. Jones, C. A. Davis, P. A. Harr, and M. Weissmann, 2013: The impact of Typhoon Jangmi (2008) on the midlatitude flow. Part I: Upper-level ridgebuilding and modification of the jet. *Quart. J. Roy. Meteor. Soc.,* **139,** 2148-2164.

Griffin, K. S., and L. F. Bosart, 2014: The extratropical transition of Tropical Cyclone Edisoana (1990). *Mon. Wea. Rev.,* **142,** 2772-2793.

Hakim, G. J., L. F. Bosart, and D. Keyser, 1995: The Ohio Valley wave-merger cyclogenesis event of 25-26 January 1978. Part I: Multiscale case study. *Mon. Wea. Rev.,* **123,** 2663-2692.

———, D. Keyser, and L. F. Bosart, 1996: The Ohio Valley wave merger cyclogenesis event of 25-26 January 1978. Part II: Diagnosis using quasigeostrophic potential vorticity inversion. *Mon. Wea. Rev.*, **124,** 2176-2205.

Harnik, N., E. Galanti, O. Martius, and O. Adam, 2014: The anomalous merging of the African and North Atlantic jet streams during Northern Hemisphere winter of 2010. *J. Climate*, **27,** 7319-7334.

Hoskins, B. J., M. E. McIntyre, and A. W. Robertson, 1985: On the use and significance of isentropic potential vorticity maps. *Quart. J. Roy. Meteor. Soc.*, **111,** 877-946.

———, and P. Berrisford, 1988: A potential vorticity perspective of the storm of 15-16 October 1987. *Weather*, **43,** 122-129.

Keyser, D., and M. A. Shapiro, 1986: A review of the structure and dynamics of upper-level frontal zones. *Mon. Wea. Rev.*, **114,** 452-499.

Knupp, K. R., T. A. Murphy, T. A. Coleman, R. A. Wade, S. A. Mullins, C. J. Schultz, E. V. Schultz, L. Carey, A. Sherrer, E. W. McCaul Jr., B. Carcione, S. Latimer, A. Kula, K. Laws, P. T. Marsh, and K. Klockow, 2014: Meteorological overview of the devastating 27 April 2011 Tornado Outbreak. *Bull. Amer. Meteor. Soc.,* **95,** 1041-1062.

Koteswaram, P., 1953: An analysis of the high tropospheric wind circulation over India in winter. *Indian J. Meteor. Geophys.*, **4,** 13-21.

———, and S. Parthasarathy, 1954: The mean jet stream over Indian in the pre-monsoon and post-monsoon seasons and vertical motions associated with subtropical jet streams. *Indian J. Meteor. Geophys.*, **5,** 138-156.

Krishnamurti, T. N., 1961: The subtropical jet stream of winter. *J. Meteor.*, **18,** 172-191.

Lai, C.-C., and L. F. Bosart, 1988: A case study of trough merger in split westerly flow. *Mon. Wea. Rev.,* **116,** 1838-1856.

Lang, A. A., and J. E. Martin, 2012: The structure and evolution of lower stratospheric frontal zones. Part I: Examples in northwesterly and southwesterly flow. *Quart. J. Roy. Meteor. Soc.*, **138,** 1350-1365.

———, and ———, 2013: The structure and evolution of lower stratospheric frontal zones. Part II: The influence of tropospheric convection on lower stratospheric frontal development. *Quart. J. Roy. Meteor. Soc.*, **139,** 1798-1809.

Lee, S., and H.-K. Kim, 2003: The dynamical relationship between subtropical and eddy-driven jets. *J. Atmos. Sci.*, **60,** 1490-1503.

Loewe, F. and V. Radok, 1950: A meridional aerological cross section in the southwest Pacific. *J. Meteor.*, **7,** 58-65.

Martin, J. E., 2014: Quasi-geostrophic diagnosis of the influence of vorticity advection on the development of upper level jet-front systems. *Quart. J. Roy. Meteor. Soc.*, in press.

Martius, O., C. Schwiertz, and H. C. Davies, 2010: Tropopause-level waveguides. *J. Atmos. Sci.,* **67,** 866-879.

Mohri, K., 1953: On the fields of wind and temperature over Japan and adjacent waters during winter of 1950-1951. *Tellus*, **5,** 340-358.

Moore, B. J., P. J. Neiman, F. M. Ralph, and F. E. Barthold, 2012: Physical processes associated with heavy flooding rainfall in Nashville, Tennessee, and vicinity during 1-2 May 2010: The role of an atmospheric river and mesoscale convective systems. *Mon. Wea. Rev.*, **140,** 358-378.

Morgan, M. C., and J. W. Nielsen-Gammon, 1998: Using tropopause maps to diagnose midlatitude weather systems. *Mon. Wea. Rev.*, **126,** 241-265.

Namias, J., and P. F. Clapp, 1949: Confluence theory of the high tropospheric jet stream. *J. Meteor.*, **6,** 330-336.

National Weather Service, cited 2014: December 18-19, 2009 winter storm. [Available online at http://www4.ncsu.edu/~nwsfo/storage/cases/20091218/.]

Newton, C. W., 1954: Frontogenesis and frontolysis as a three-dimensional process. *J. Meteor.,* **11,** 449-461.

O'Rourke, A. K., and G. K. Vallis, 2013: Jet interaction and the influence of a minimum phase speed bound on the propagation of eddies. *J. Atmos. Sci.*, **70,** 2614-2628.

Palmén, E., and C. W. Newton, 1948: A study of the mean wind and temperature distribution in the vicinity of the polar front in winter. *J. Meteor.*, **5,** 220-226.

———, and ———, 1969: *Atmospheric Circulation Systems: Their Structure and Physical Interpretation*. Academic Press, 603 pp.

Riehl, H., 1962: Jet streams of the atmosphere. Dept. of Atmospheric Science Tech. Rep. 32, Colorado State University, Fort Collins, CO, 117 pp.

Rolph, G. D., 2015: Real-time Environmental Applications and Display sYstem (READY) Website (http://ready.arl.noaa.gov). NOAA Air Resources Laboratory, Silver Spring, MD.

Saha, S. and 51 co-authors, 2010: The NCEP Climate Forecast System Reanalysis. *Bull. Amer. Meteor. Soc.*, **91,** 1015-1057.

Sawyer, J. S., 1956: The vertical circulation at meteorological fronts and its relation to frontogenesis. *Proc. Roy. Soc. London,* **234A,** 346-362.

Shapiro, M. A., 1982: Mesoscale weather systems of the central United States. CIRES, 78 pp.

———, and D. Keyser, 1990: Fronts, jet streams, and the tropopause. *Extratropical Cyclones: The Erik Palmén Memorial Volume,* C. Newton and E. O. Holopainen, Eds., Amer. Meteor. Soc., 167-191.

———, H. Wernli, J.-W. Bao, J. Methven, X. Zou, J. Doyle, T. Holt, E. Donall-Grell, and P. Neiman, 1999: A planetary-scale to mesoscale perspective of the life cycles of extratropical cyclones: The bridge between theory and observations. *The Life Cycles of Extratropical Cyclones*, M. Shapiro and S. Grønås, Eds., Amer. Meteor. Soc., 139-185.

Son, S.-W., and S. Lee, 2005: The response of westerly jets to thermal driving in a primitive equation model. *J. Atmos. Sci.,* **62,** 3741-3757.

Strahl, J. L. S., and P. J. Smith, 2001: A diagnostic study of an explosively developing extratropical cyclone and an associated 500-hPa trough merger. *Mon. Wea. Rev.,* **129,** 2310-2328.

Sutcliffe, R. C., 1947: A contribution to the problem of development. *Quart. J. Roy. Meteor. Soc.*, **73,** 370-383.

———, and J. K. Bannon, 1954: Seasonal changes in the upper-air conditions in the Mediterranean Middle East area. *Proc. Int. Association of Meteorology*, Rome, Italy, Int. Union of Geodesy and Geophysics. 322-334.

Winters, A. C., and J. E. Martin, 2014: The role of a polar/subtropical jet superposition in the May 2010 Nashville Flood. *Wea. Forecasting*, **29,** 954-974.

Yeh, T. C., 1950: The circulation of the high tropopause over China in the winter of 1945-46. *Tellus*, **2,** 173-183.

Figure Captions

Fig. 1. Mean meridional cross section of potential temperature for 1 Jan 1956 with the polar, subtropical, and tropical tropopauses labeled as indicated in the legend. The polar frontal layer is shaded in gray. (Modified from DT57, Fig. 13.)

Fig. 2. Northern Hemispheric map of tropopause height (hPa) at 0300 UTC 1 Jan 1956. Tropopause breaks that correspond to the subtropical (STJ) and polar jet (POLJ) are labeled accordingly. The area identified with a circle is a region characterized by a vertical superposition of the polar and subtropical jets. Darkest shading corresponds to the polar tropopause, white shading to the subtropical tropopause, and light gray to the tropical tropopause.

Fig. 3. (a) The 300 hPa wind speeds (shaded every 10 m s^{-1} starting at 30 m s^{-1}) at 0000 UTC 27 Apr 2010 depicting separate polar and subtropical jets. (b) Cross section A-A', in Fig. 3a, through separate polar and subtropical jet cores with contours of 1-,2-, and 3-PVU (black); 4- ,5- ,6- ,7- ,8-, and 9-PVU (light gray); potential temperature every 5 K (dashed gray); and wind speed every 10 m s^{-1} beginning at 30 m s^{-1} (dark gray). The 315-330- and 340-355-K isentropic layers, used to identify the locations of the jets, are shaded gray. The dark vertical lines correspond to grid columns with the black dot confirming a positive identification of a polar or subtropical jet. (c) As in (a), but for a superposed jet at 0000 UTC 24 Oct 2010. (d) As in (b), but for the cross section B-B', in Fig. 3c, with two positive identifications (black dots) within a single grid column indicating a jet superposition.

Fig. 4. Idealized configurations of jet circulations associated with a straight jet streak on an isobaric surface in the upper troposphere. Geopotential height (thick solid lines), potential temperature (dashed lines), geostrophic wind speed (fill pattern; with the jet speed maximum represented by the J), and Sawyer-Eliassen vertical motions indicated by “up” and “down” for a regime of (a) no geostrophic temperature advection, (b) upper-tropospheric geostrophic cold-air advection, and (c) upper-tropospheric geostrophic warm-air advection along the jet axis. [From Fig. 3 in Lang and Martin (2012).]

Fig. 5. Accumulated snowfall in cm during the period 18-20 December 2009 over the Mid-Atlantic and Northeastern United States. [Modified from NOAA HPC; National Weather Service 2014].

Fig. 6. [left column] 250 hPa wind speed is shaded with the gray fill pattern every 10 m s^{-1} beginning at 30 m s^{-1}, 250 hPa geopotential heights are contoured in red every 120 m, sea level pressure is contoured with the dashed black lines every 4 hPa below 1000 hPa, the location of the sea-level pressure minimum is identified with the red “L”, and jet axes are identified as specified in the legend for (a) 0000 UTC 19 December 2009, (c) 1800 UTC 19 December 2009, and (e) 1200 UTC 20 December 2009. [right column] Cross sections, as identified in the plot immediately to its left, of wind speed shaded every 10 m s^{-1} beginning at 30 m s^{-1} (blue fill pattern), potential temperature contoured every 5 K (dashed green lines), and contours of 1-,2-, and 3-PVU (black) at (b) 0000 UTC 19 December 2009, (d) 1800 UTC 19 December 2009, and (f) 1200 UTC 20 December 2009. The gray shaded isentropic layers are those used to identify

the jet axes using the scheme outlined in the text and the 320-K and 325-K isentropes are highlighted with the dashed red lines in the cross sections for reasons discussed in the text.

Fig. 7. [left column] 200 hPa geopotential height is contoured in red every 120 m, 200 hPa geostrophic wind speed is shaded with the gray fill pattern every 10 m s^{-1} beginning at 30 m s^{-1}, positive perturbation pressure depths within the 340-355-K isentropic layer are shaded in the green fill pattern every 10 hPa, and the subtropical jet axis is identified with the thick, dashed red line for (a) 0000 UTC 19 December 2009, (c) 1800 UTC 19 December 2009, and (e) 1200 UTC 20 December 2009. [right column] Infrared satellite imagery from University of Wisconsin – CIMSS for (b) 0000 UTC 19 December 2009, (d) 1800 UTC 19 December 2009, and (f) 1200 UTC 20 December 2009. The yellow box denotes the source region for the trajectories shown in Fig. 8.

Fig. 8. 72 h forward trajectories initialized at 1200 UTC 18 December 2009 within the yellow box (5^{o}N–10^{o}N; 85^{o}W–90^{o}W) over the eastern equatorial Pacific Ocean shown in Fig. 7b. Trajectories were initialized at 3000 m AGL within the NOAA HYSPLIT model and projected forward using archived GDAS data. The bottom panel depicts the potential temperature of the trajectories throughout the duration of the simulation.

Fig. 9. 250 hPa geostrophic wind speed is shaded with the gray fill pattern every 20 m s^{-1} beginning at 40 m s^{-1}, 300 hPa geostrophic cold (warm) air advection is shaded in the blue (red) fill pattern every 4 (-4)$x10^{-4}$ K s^{-1}, 500 hPa potential temperature is contoured in red every 3 K, and sea level pressure is contoured with the dashed black lines every 4 hPa below 1000 hPa for

(a) 0000 UTC 19 December 2009, (b) 1800 UTC 19 December 2009, and (c) 1200 UTC 20 December 2009. The polar (subtropical) jet axis is indicated by the thick, dashed blue (red) line, the yellow circle highlights the region of jet superposition, and the red “L” marks the location of the sea level pressure minimum.

Fig. 10. Cross sections, as indicated in Fig. 9, of Sawyer-Eliassen streamfunction every 300 m hPa s^{-1} with negative (positive) values contoured with dashed (solid) black lines, potential temperature every 5 K contoured in red, positive omega associated with the Sawyer-Eliassen circulation shaded in the purple fill pattern every 1 dPa s^{-1} beginning at 1 dPa s^{-1}, geostrophic wind speeds shaded with the gray fill pattern every 10 m s^{-1} beginning at 30 m s^{-1}, and the 1.5-PVU surface identified by the bold blue line. The sense of the circulation is depicted by the arrowheads plotted on the streamfunction contours. The 320 K and 325 K isentropes are bolded in (b) for reasons discussed in the text.

Fig. 11. The 48 h precipitation estimates (shaded; mm; following the color bar) for 0000 UTC 1 May – 0000 UTC 3 May 2010 from the National Precipitation Verification Unit quantitative precipitation estimates product. The location of Nashville (BNA), Memphis (MEM), and Jackson (MKL) are identified. [From Moore et al. (2012, their Fig. 2).]

Fig. 12. Conventions identical to Fig. 6 but for (a,b) 0000 UTC 1 May 2010, (c,d) 1200 UTC 1 May 2010, and (e,f) 0000 UTC 2 May 2010. Precipitation at 1200 UTC 1 May 2010 in (c) is denoted by the green fill pattern and sea level pressure is now contoured every 4 hPa below 996 hPa in the left column.

Fig. 13. 300 hPa geostrophic wind speed is shaded in the gray fill pattern every 20 m s^{-1} beginning at 40 m s^{-1}, 300 hPa geostrophic cold (warm) air advection is shaded in the blue (red) fill pattern every 4 (-4)x10^{-4} K s^{-1}, and 400 hPa potential temperature is contoured in red every 3 K at (a) 0000 UTC 1 May 2010, (b) 1200 UTC 1 May 2010, and (c) 0000 UTC 2 May 2010. Polar jet axes are indicated by the thick, blue dashed line and the yellow circle highlights the region of jet superposition.

Fig. 14. Conventions are identical to those in Fig. 10, but for the cross section shown in Fig. 13a.

Fig. 15. 200 hPa velocity potential contoured every 3x10^{6} m^{2} s^{-1} with positive (negative) values identified with solid (dashed) thick red lines, the 1-, 2-, and 3-PVU contours at 300 hPa (200 hPa) are identified with the thin blue (red) lines, and negative PV advection within the 1-3 PVU channel by the divergent winds (arrows) at 200 hPa are shaded in the green fill pattern every 2x10^{-5} PVU s^{-1} at (a) 0000 UTC 1 May 2010, (b) 1200 UTC 1 May 2010, and (c) 0000 UTC 2 May 2010.

Figures

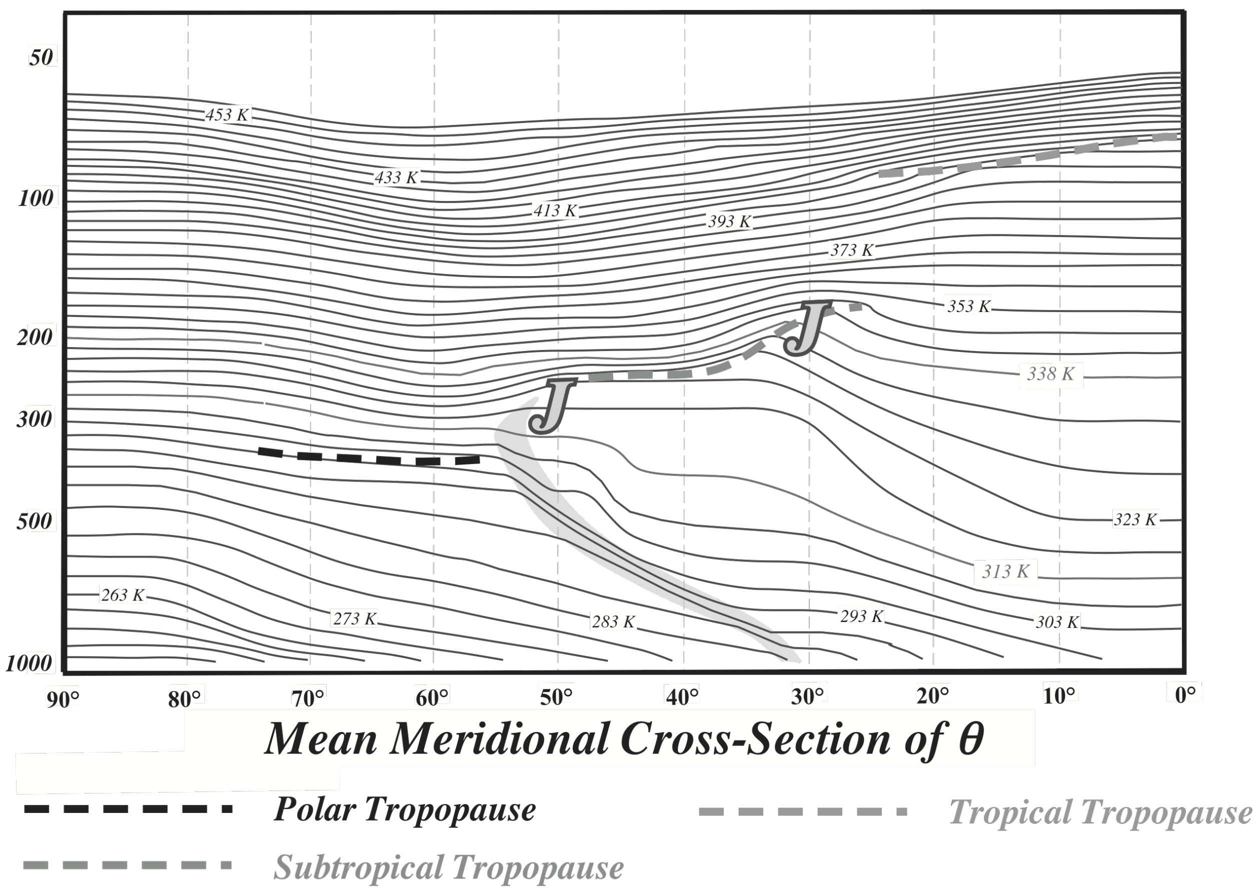

FIG 1. Mean meridional cross section of potential temperature for 1 Jan 1956 with the polar, subtropical, and tropical tropopauses labeled as indicated in the legend. The polar frontal layer is shaded in gray. (Modified from DT57, Fig. 13.)

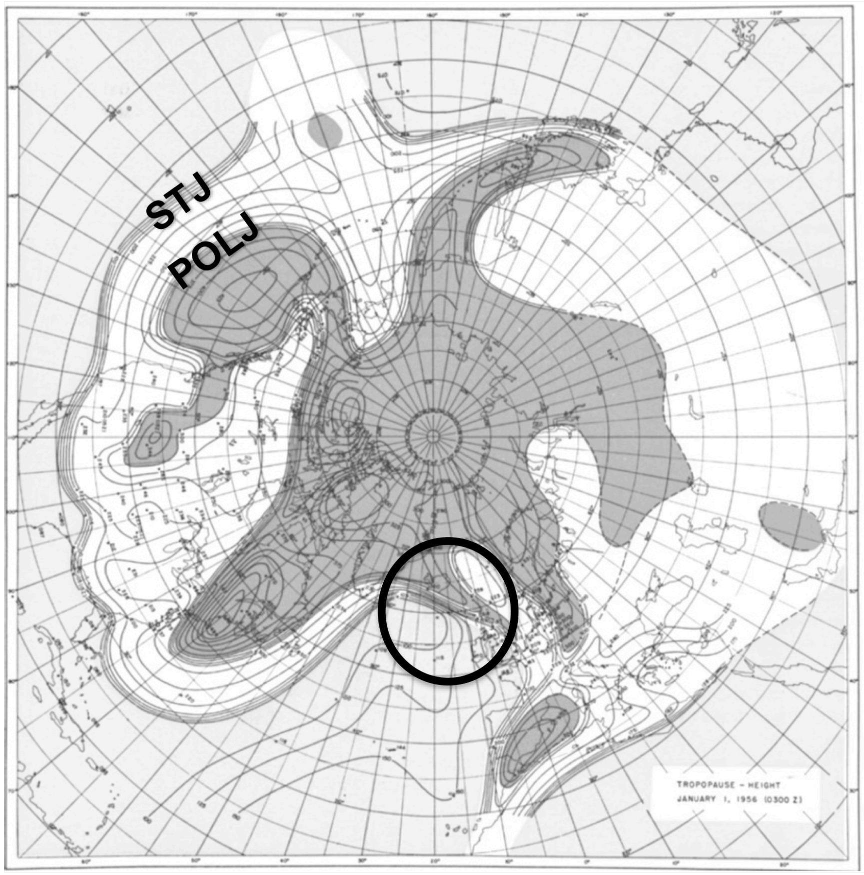

FIG 2. Northern Hemispheric map of tropopause height (hPa) at 0300 UTC 1 Jan 1956. Tropopause breaks that correspond to the subtropical (STJ) and polar jet (POLJ) are labeled accordingly. The area identified with a circle is a region characterized by a vertical superposition of the polar and subtropical jets. Darkest shading corresponds to the polar tropopause, white shading to the subtropical tropopause, and light gray to the tropical tropopause.

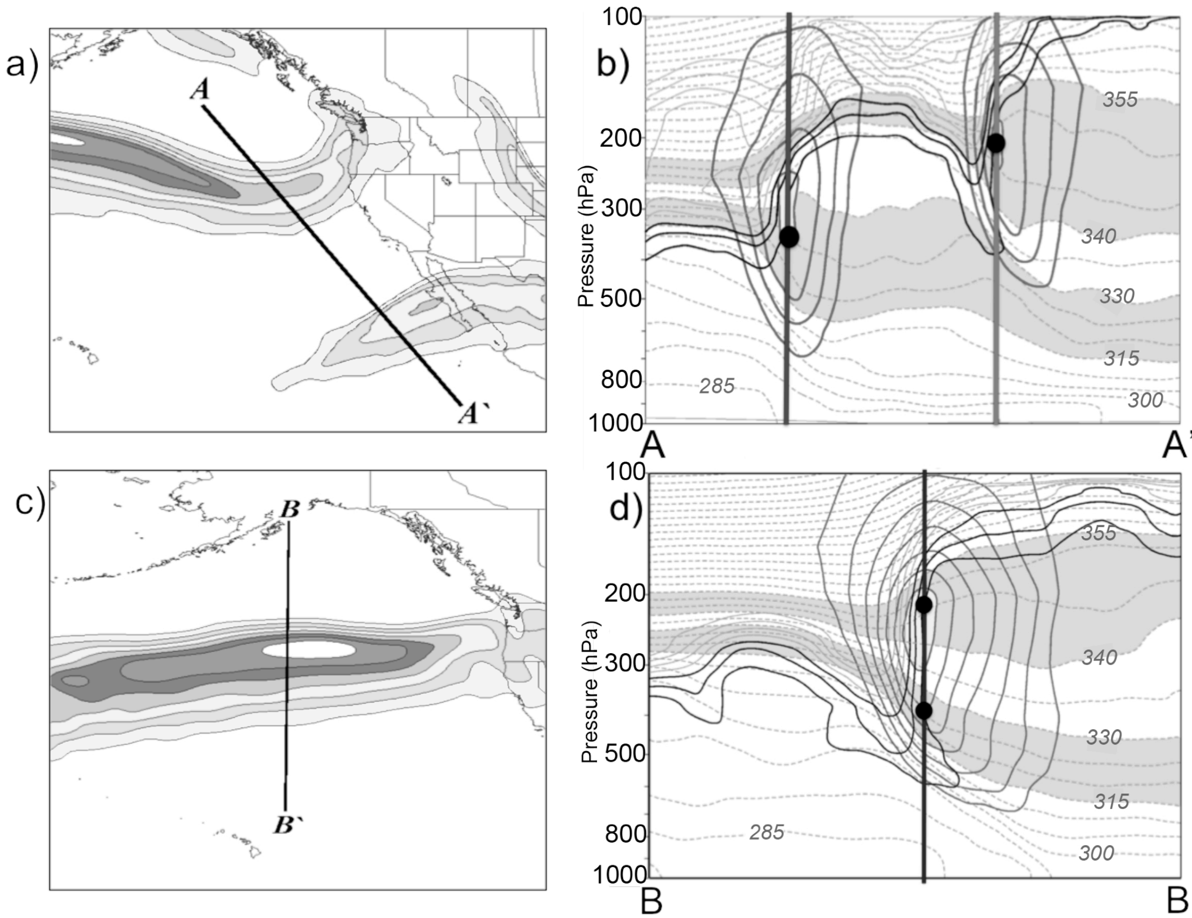

FIG. 3. (a) The 300 hPa wind speeds (shaded every 10 m s^{-1} starting at 30 m s^{-1}) at 0000 UTC 27 Apr 2010 depicting separate polar and subtropical jets. (b) Cross section A-A', in Fig. 3a, through separate polar and subtropical jet cores with contours of 1-,2-, and 3-PVU (black); 4- ,5- ,6- ,7- ,8-, and 9-PVU (light gray); potential temperature every 5 K (dashed gray); and wind speed every 10 m s^{-1} beginning at 30 m s^{-1} (dark gray). The 315-330- and 340-355-K isentropic layers, used to identify the locations of the jets, are shaded gray. The dark vertical lines correspond to grid columns with the black dot confirming a positive identification of a polar or subtropical jet. (c) As in (a), but for a superposed jet at 0000 UTC 24 Oct 2010. (d) As in (b), but for the cross section B-B', in Fig. 3c, with two positive identifications (black dots) within a single grid column indicating a jet superposition.

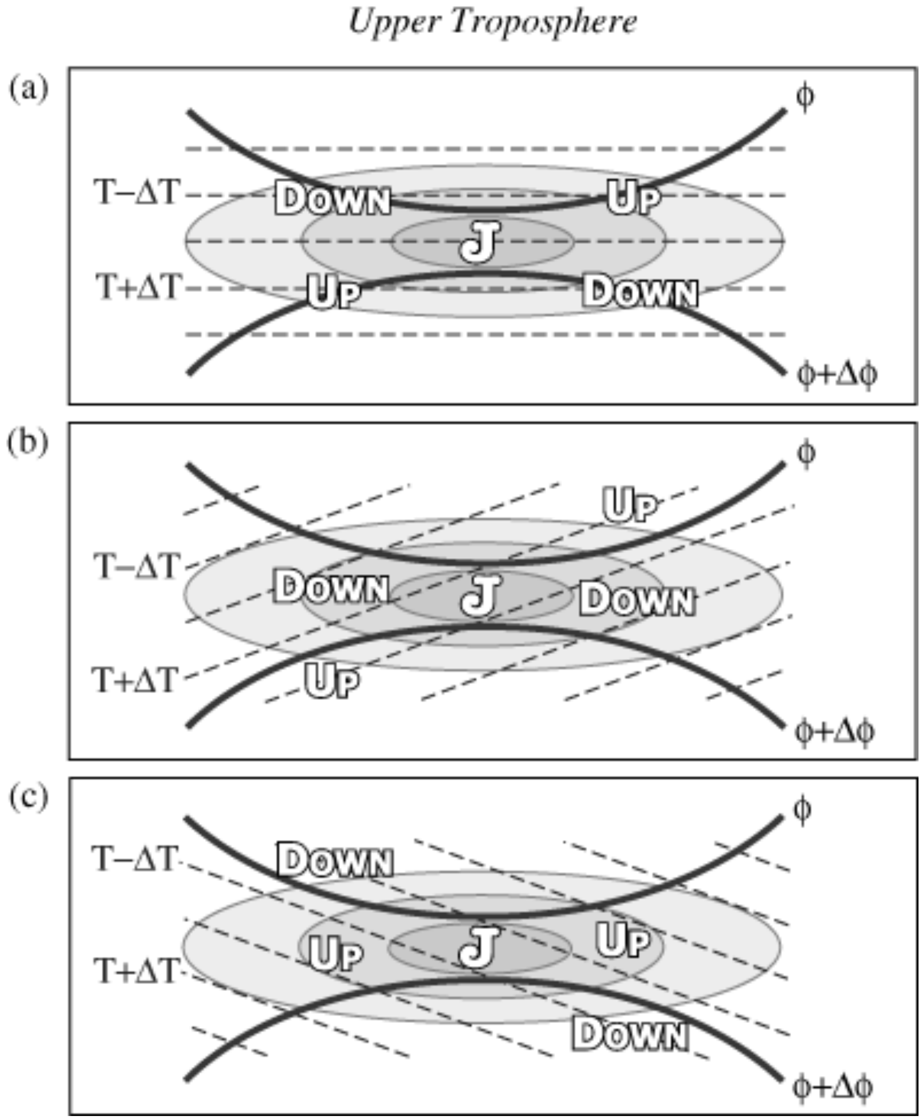

FIG. 4. Idealized configurations of jet circulations associated with a straight jet streak on an isobaric surface in the upper troposphere. Geopotential height (thick solid lines), potential temperature (dashed lines), geostrophic wind speed (fill pattern; with the jet speed maximum represented by the J), and Sawyer-Eliassen vertical motions indicated by "up" and "down" for a regime of (a) no geostrophic temperature advection, (b) upper-tropospheric geostrophic cold-air advection, and (c) upper-tropospheric geostrophic warm-air advection along the jet axis. [From Fig. 3 in Lang and Martin (2012).]

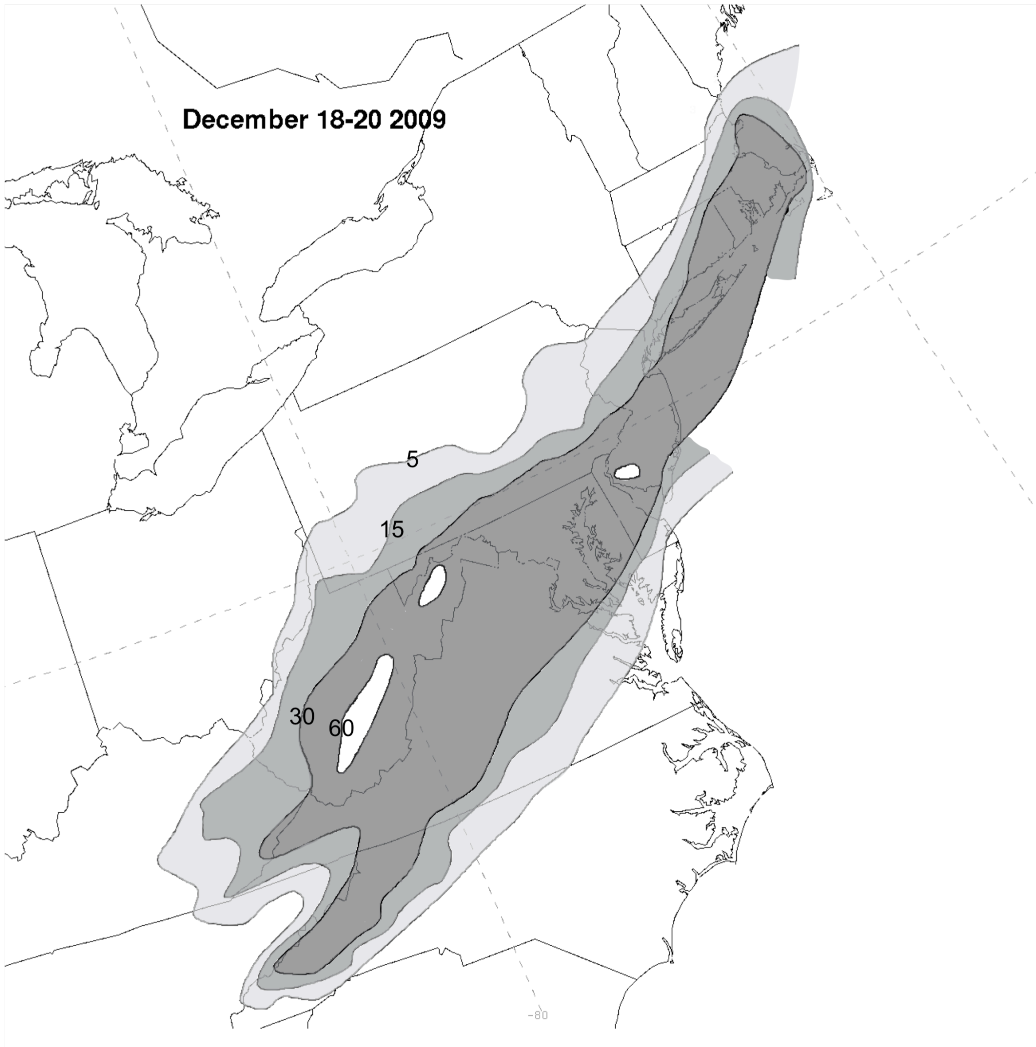

FIG. 5. Accumulated snowfall in cm during the period 18-20 December 2009 over the Mid-Atlantic and Northeastern United States. [Modified from NOAA HPC; National Weather Service 2014].

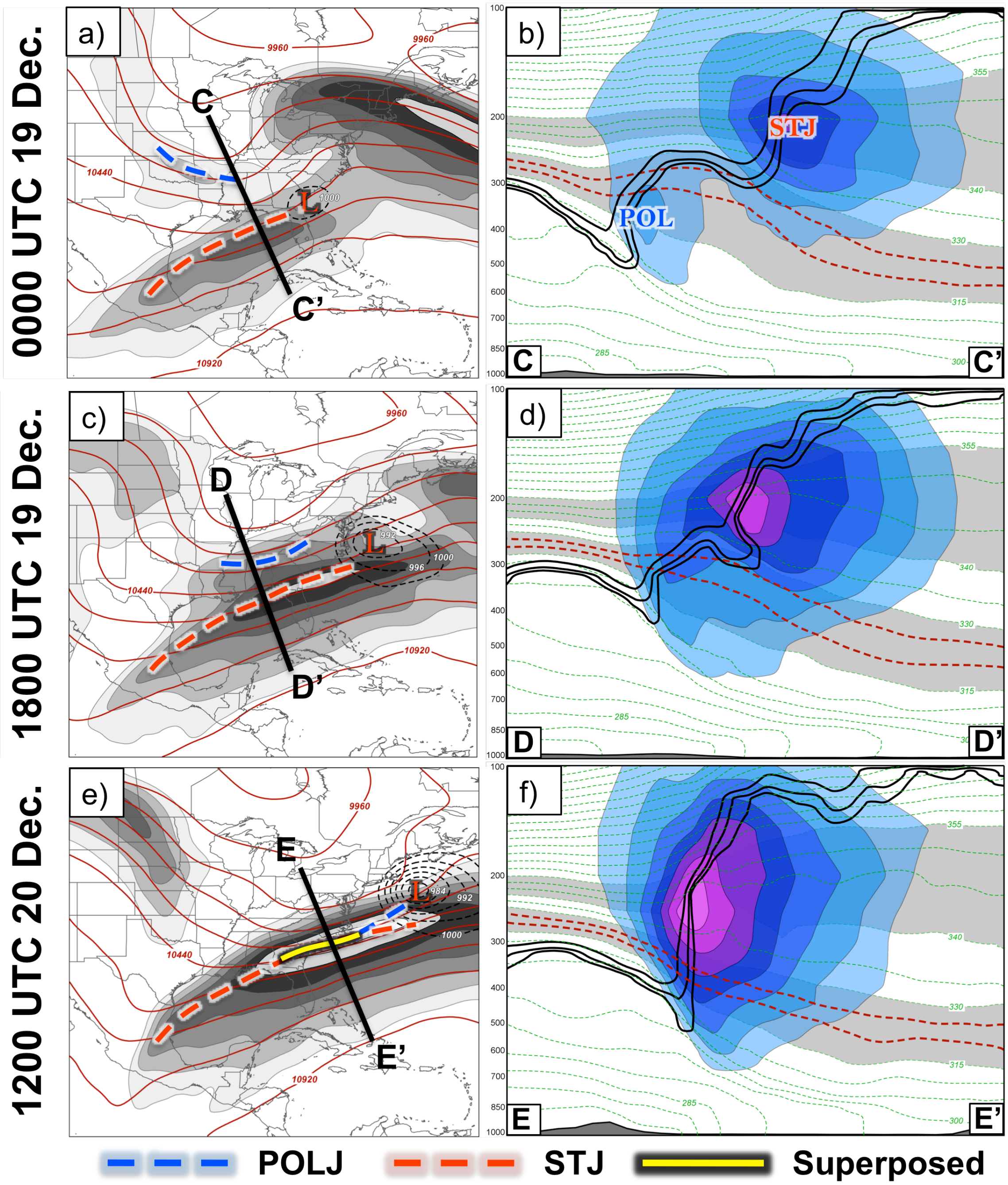

FIG. 6. [left column] 250 hPa wind speed is shaded with the gray fill pattern every 10 m s^{-1} beginning at 30 m s^{-1}, 250 hPa geopotential heights are contoured in red every 120 m, sea level pressure is contoured with the dashed black lines every 4 hPa below 1000 hPa, the location of the sea-level pressure minimum is identified with the red “L”, and jet axes are identified as specified in the legend for (a) 0000 UTC 19 December 2009, (c) 1800 UTC 19 December 2009, and (e) 1200 UTC 20 December 2009. [right column] Cross sections, as identified in the plot immediately to its left, of wind speed shaded every 10 m s^{-1} beginning at 30 m s^{-1} (blue fill pattern), potential temperature contoured every 5 K (dashed green lines), and contours of 1-,2-, and 3-PVU (black) at (b) 0000 UTC 19 December 2009, (d) 1800 UTC 19 December 2009, and (f) 1200 UTC 20 December 2009. The gray shaded isentropic layers are those used to identify the jet axes using the scheme outlined in the text and the 320-K and 325-K isentropes are highlighted with the dashed red lines in the cross sections for reasons discussed in the text.

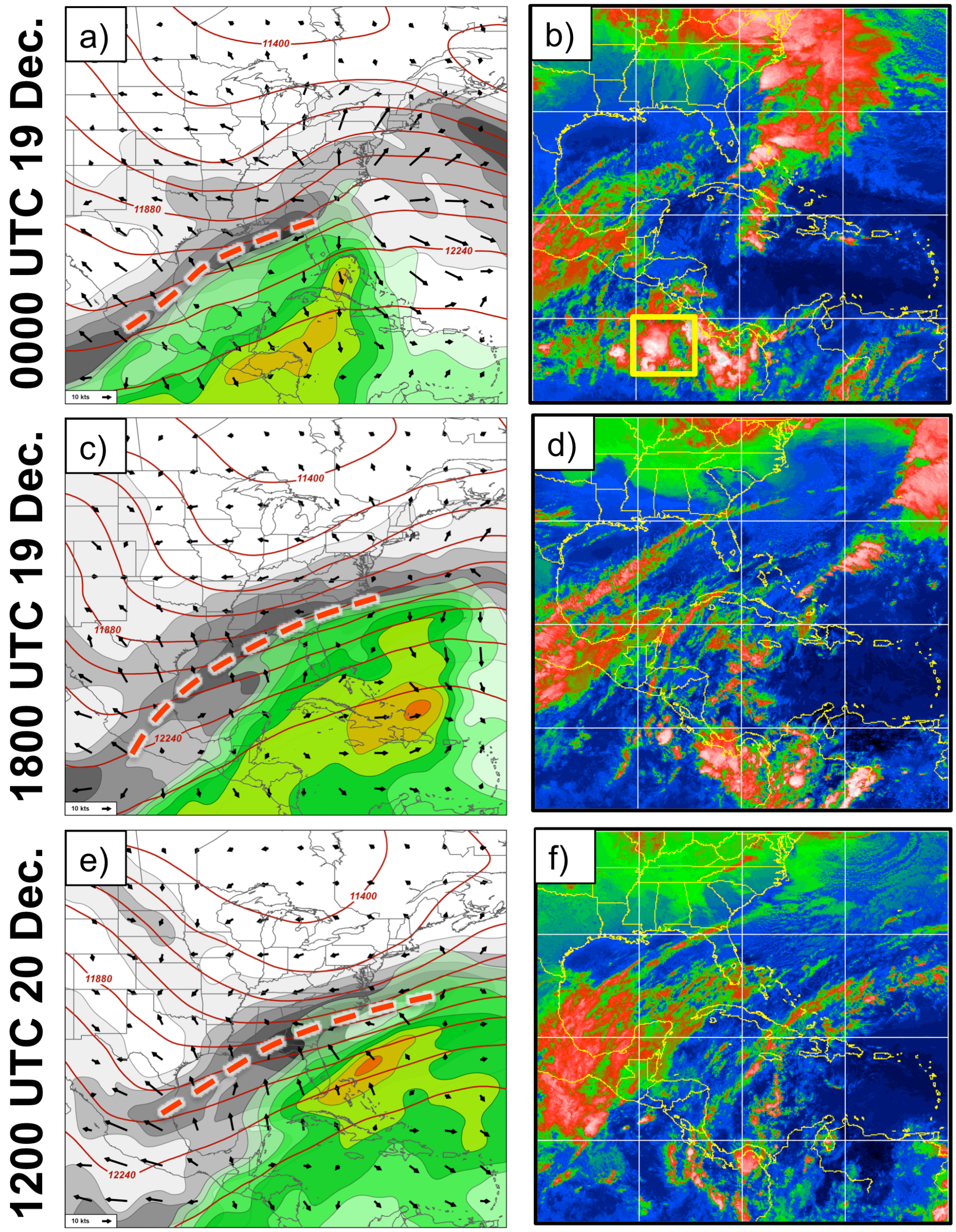

FIG. 7. [left column] 200 hPa geopotential height is contoured in red every 120 m, 200 hPa geostrophic wind speed is shaded with the gray fill pattern every 10 m s^{-1} beginning at 30 m s^{-1}, positive perturbation pressure depths within the 340-355-K isentropic layer are shaded in the green fill pattern every 10 hPa, and the subtropical jet axis is identified with the thick, dashed red line for (a) 0000 UTC 19 December 2009, (c) 1800 UTC 19 December 2009, and (e) 1200 UTC 20 December 2009. [right column] Infrared satellite imagery from University of Wisconsin – CIMSS for (b) 0000 UTC 19 December 2009, (d) 1800 UTC 19 December 2009, and (f) 1200 UTC 20 December 2009. The yellow box denotes the source region for the trajectories shown in Fig. 8.

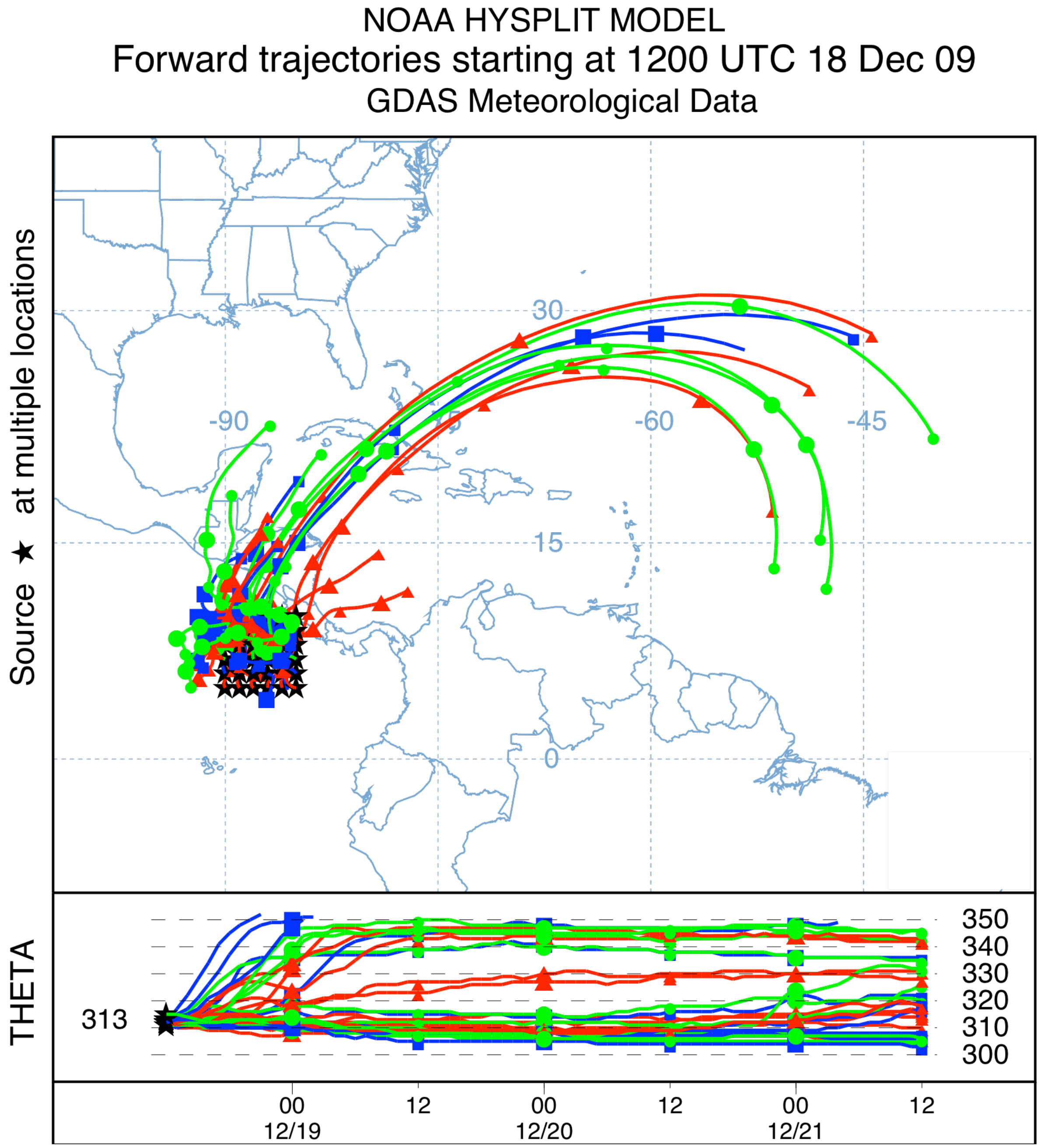

FIG. 8. 72 h forward trajectories initialized at 1200 UTC 18 December 2009 within the yellow box (5°N–10°N; 85°W–90°W) over the eastern equatorial Pacific Ocean shown in Fig. 7b. Trajectories were initialized at 3000 m AGL within the NOAA HYSPLIT model and projected forward using archived GDAS data. The bottom panel depicts the potential temperature of the trajectories throughout the duration of the simulation.

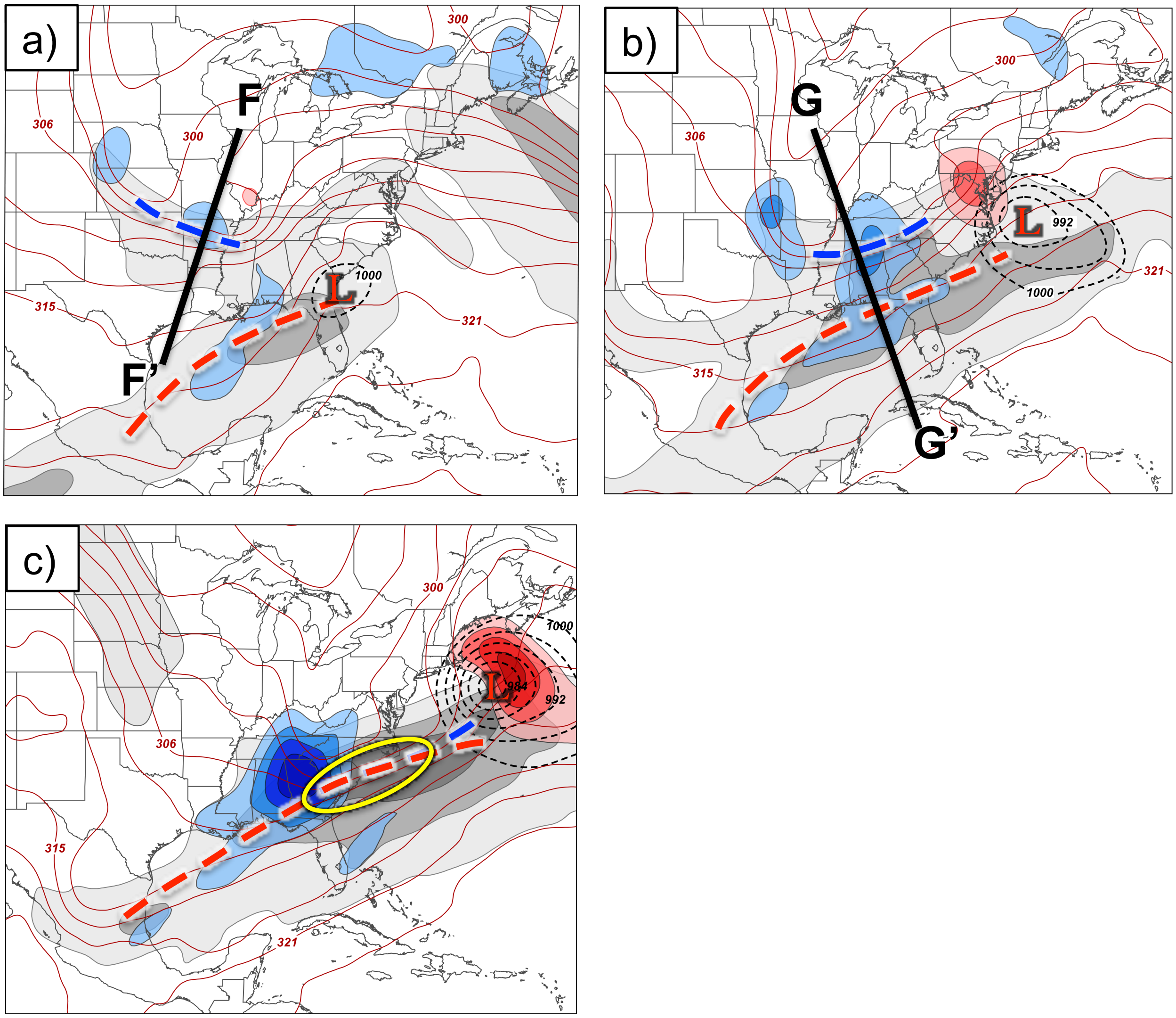

FIG. 9. 250 hPa geostrophic wind speed is shaded with the gray fill pattern every 20 m s^{-1} beginning at 40 m s^{-1}, 300 hPa geostrophic cold (warm) air advection is shaded in the blue (red) fill pattern every 4 (-4)x10^{-4} K s^{-1}, 500 hPa potential temperature is contoured in red every 3 K, and sea level pressure is contoured with the dashed black lines every 4 hPa below 1000 hPa for (a) 0000 UTC 19 December 2009, (b) 1800 UTC 19 December 2009, and (c) 1200 UTC 20 December 2009. The polar (subtropical) jet axis is indicated by the thick, dashed blue (red) line, the yellow circle highlights the region of jet superposition, and the red "L" marks the location of the sea level pressure minimum.

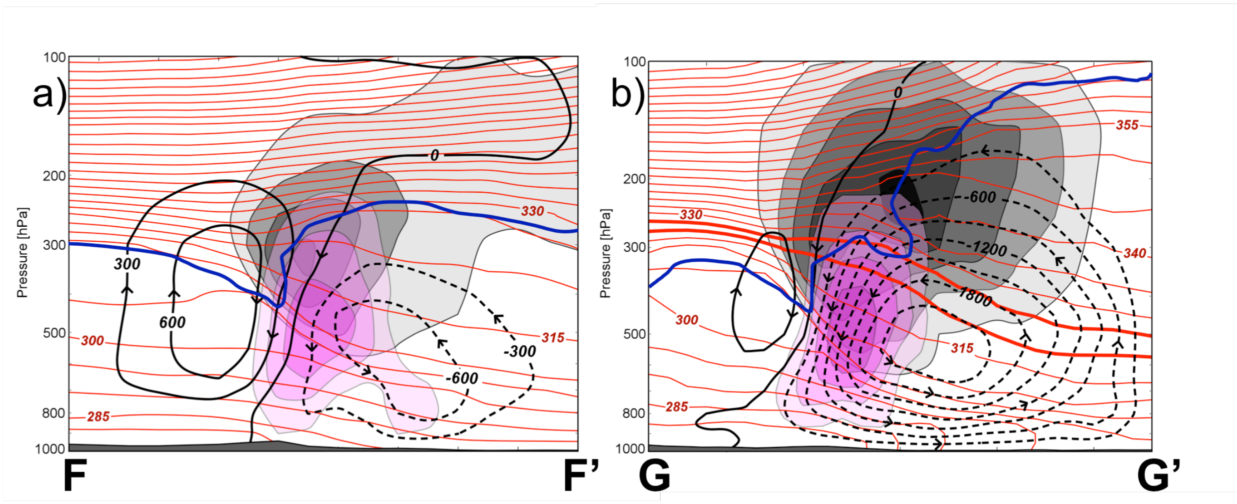

FIG. 10. Cross sections, as indicated in Fig. 9, of Sawyer-Eliassen streamfunction every 300 m hPa s^{-1} with negative (positive) values contoured with dashed (solid) black lines, potential temperature every 5 K contoured in red, positive omega associated with the Sawyer-Eliassen circulation shaded in the purple fill pattern every 1 dPa s^{-1} beginning at 1 dPa s^{-1}, geostrophic wind speeds shaded with the gray fill pattern every 10 m s^{-1} beginning at 30 m s^{-1}, and the 1.5-PVU surface identified by the bold blue line. The sense of the circulation is depicted by the arrowheads plotted on the streamfunction contours. The 320 K and 325 K isentropes are bolded in (b) for reasons discussed in the text.

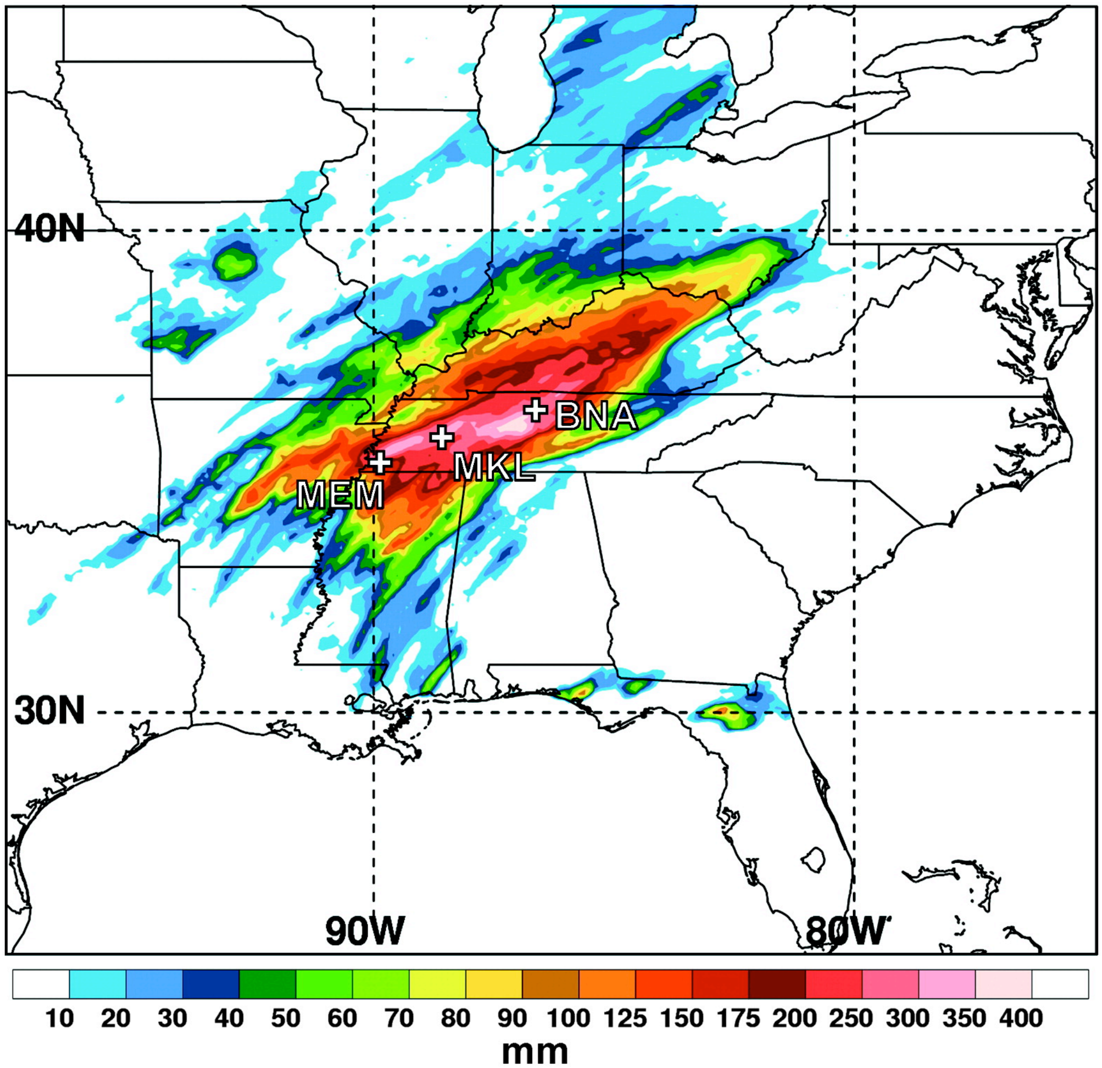

FIG. 11. The 48 h precipitation estimates (shaded; mm; following the color bar) for 0000 UTC 1 May – 0000 UTC 3 May 2010 from the National Precipitation Verification Unit quantitative precipitation estimates product. The location of Nashville (BNA), Memphis (MEM), and Jackson (MKL) are identified. [From Moore et al. (2012, their Fig. 2).]

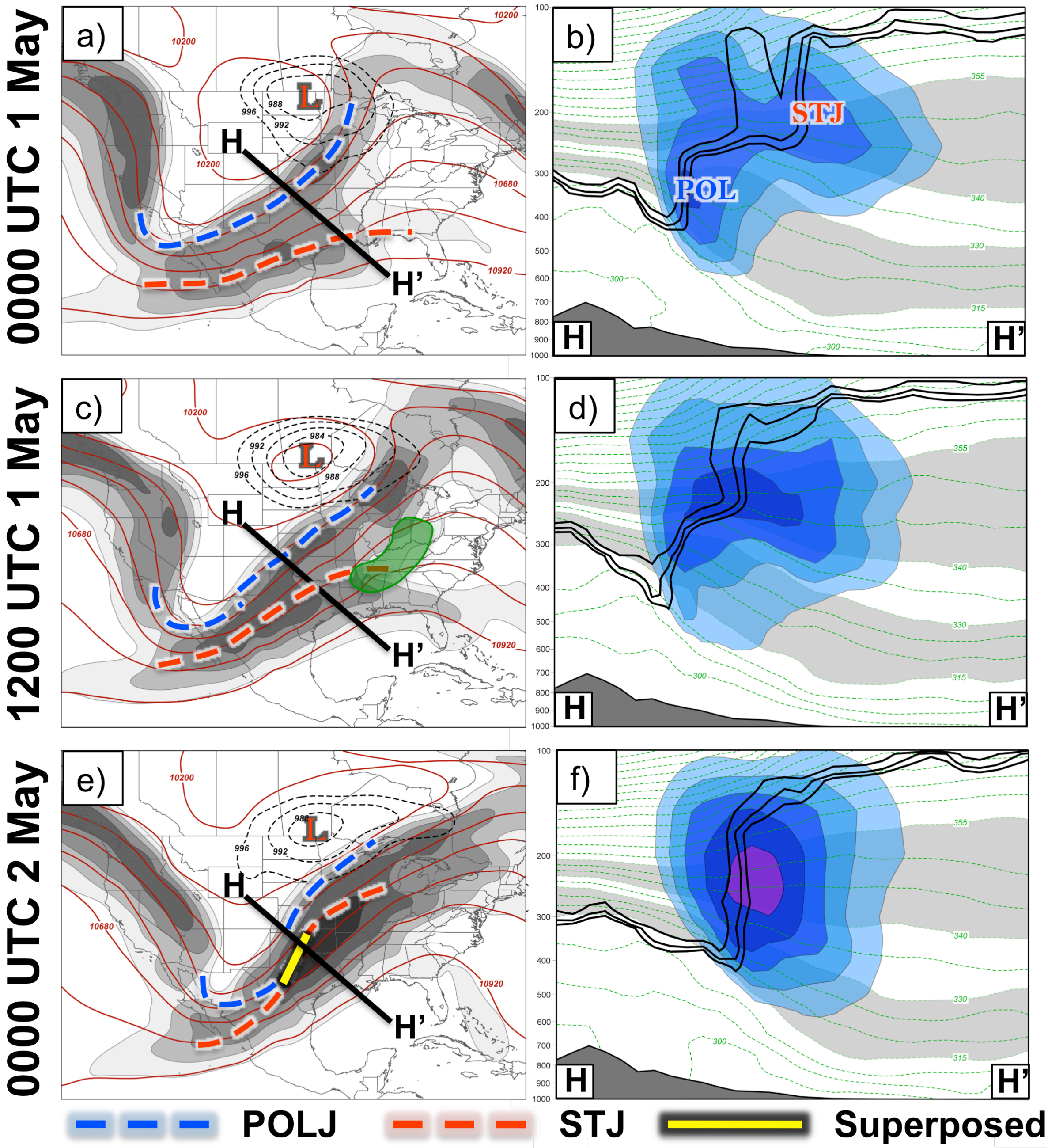

FIG. 12. Conventions identical to Fig. 6 but for (a,b) 0000 UTC 1 May 2010, (c,d) 1200 UTC 1 May 2010, and (e,f) 0000 UTC 2 May 2010. Precipitation at 1200 UTC 1 May 2010 in (c) is denoted by the green fill pattern and sea level pressure is now contoured every 4 hPa below 996 hPa in the left column.

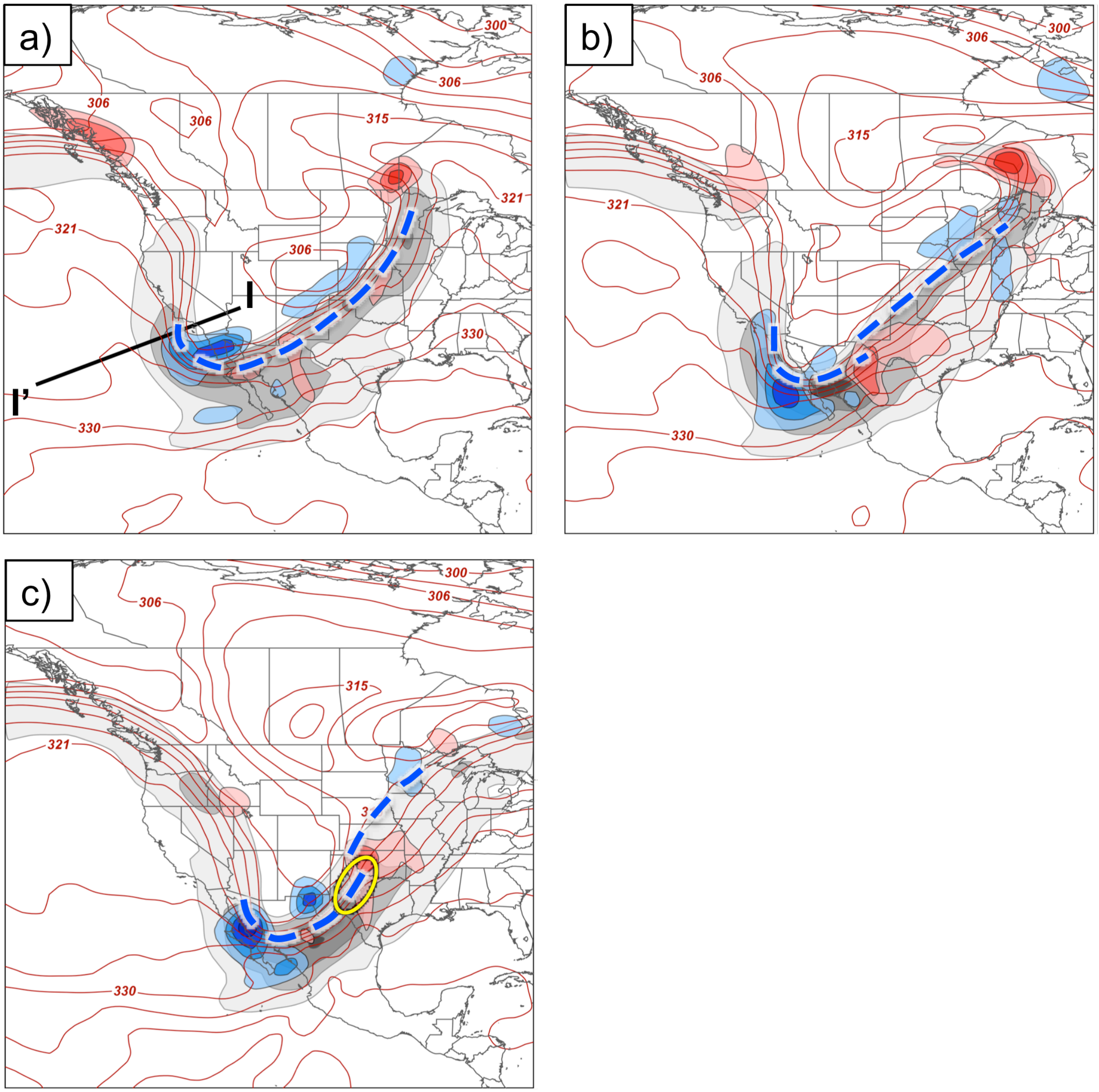

FIG. 13. 300 hPa geostrophic wind speed is shaded in the gray fill pattern every 20 m s^{-1} beginning at 40 m s^{-1}, 300 hPa geostrophic cold (warm) air advection is shaded in the blue (red) fill pattern every 4 (-4)x10^{-4} K s^{-1}, and 400 hPa potential temperature is contoured in red every 3 K at (a) 0000 UTC 1 May 2010, (b) 1200 UTC 1 May 2010, and (c) 0000 UTC 2 May 2010. Polar jet axes are indicated by the thick, blue dashed line and the yellow circle highlights the region of jet superposition.

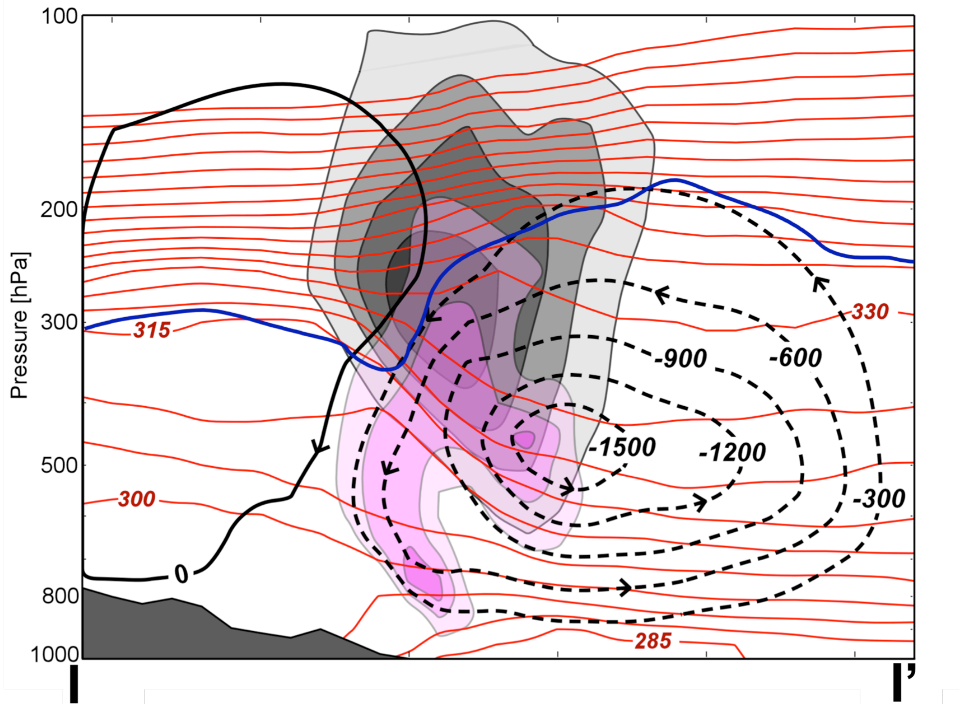

FIG. 14. Conventions are identical to those in Fig. 10, but for the cross section shown in Fig. 13a.

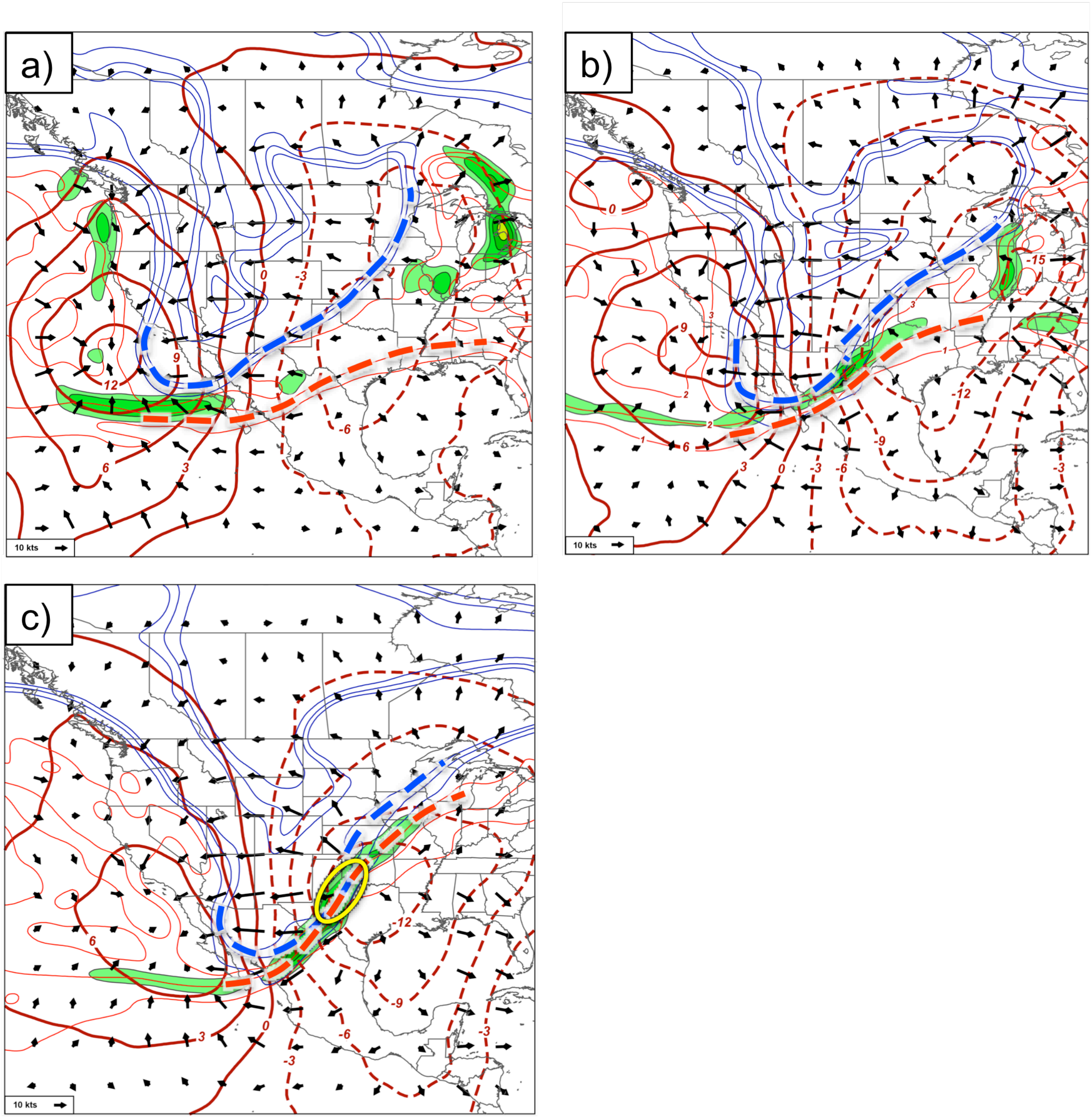

FIG. 15. 200 hPa velocity potential contoured every 3×10^{6} m^{2} s^{-1} with positive (negative) values identified with solid (dashed) thick red lines, the 1-, 2-, and 3-PVU contours at 300 hPa (200 hPa) are identified with the thin blue (red) lines, and negative PV advection within the 1-3 PVU channel by the divergent winds (arrows) at 200 hPa are shaded in the green fill pattern every 2×10^{-5} PVU s^{-1} at (a) 0000 UTC 1 May 2010, (b) 1200 UTC 1 May 2010, and (c) 0000 UTC 2 May 2010.